RSC Advances

REVIEW

View Article Online
View Journal | View Issue

Cite this: *RSC Adv.*, 2024, **14**, 8409

Yolk–shell smart polymer microgels and their hybrids: fundamentals and applications

Iqra Sajid,[a] Ahmad Hassan,[a] Robina Begum, *[a] Shuiqin Zhou,[b] Ahmad Irfan,[c] Aijaz Rasool Chaudhry[d] and Zahoor H. Farooqi *[a]

Yolk–shell microgels and their hybrids have attained great importance in modern-day research owing to their captivating features and potential uses. This manuscript provides the strategies for preparation, classification, properties and current applications of yolk–shell microgels and their hybrids. Some of the yolk–shell microgels and their hybrids are identified as smart polymer yolk–shell microgels and smart hybrid microgels, respectively, as they react to changes in particular environmental stimuli such as pH, temperature and ionic strength of the medium. This unique behavior makes them a perfect candidate for utilization in drug delivery, selective catalysis, adsorption of metal ions, nanoreactors and many other fields. This review demonstrates the contemporary progress along with suggestions and future perspectives for further research in this specific field.

Received 3rd January 2024
Accepted 26th February 2024

DOI: 10.1039/d4ra00035h

rsc.li/rsc-advances

1. Introduction

Microspheres with movable cores within the cavities of a shell are called yolk–shell microspheres (YSMs). These systems with controllable size and composition having low density, multi-functionality, and excellent loading capacity have been reported.[1–3] Owing to these properties, YSMs find potential applications in various fields such as catalysis,[4] drug delivery,[5] biomedicines,[6] lithium-ion batteries,[7] and dual-mode imaging.[8]

The colloidal dispersion of gel particles with a diameter ranging from 0.1 to 100 μm in a suitable solvent are termed as microgels.[9] Cross-linked polymeric systems that respond to a change in external stimuli are called smart microgels. Their properties of permeability, deformability, as well as uptake and release behavior can be tuned by changing their cross-linking density and the strength of external stimuli. This smart behavior makes them a perfect choice for various uses.[10–13] Microgels can be further classified into core–shell microgels,[14] Janus microgels,[15] hollow microgels[16] and yolk–shell microgels.[17,18]

Recently, yolk–shell microspheres having a movable core and cross-linked polymeric shell[19–21] have obtained considerable importance owing to their peculiar responsive behavior towards external stimuli such as temperature,[17,22] pH,[23,24] and

[a]*School of Chemistry, University of the Punjab, New Campus, Lahore 54590, Pakistan. E-mail: zhfarooqi@gmail.com; zahoor.chem@pu.edu.pk; robina.hons@pu.edu.pk; Fax: +92-42-9231269; Tel: +92-42-9230463 ext. 817*

[b]*Department of Chemistry of The College of Staten Island, PhD Program in Chemistry of The Graduate Centre, The City University of New York, 2800 Victory Boulevard, Staten Island, NY 10314, USA*

[c]*Department of Chemistry, College of Science, King Khalid University, P. O. Box 9004, Abha 61413, Saudi Arabia*

[d]*Department of Physics, College of Science, University of Bisha, P. O. Box 551, Bisha, 61922, Saudi Arabia*

Iqra Sajid

Iqra Sajid obtained her BS and M. Phil degrees in Chemistry from the School of Chemistry, University of the Punjab (PU), Lahore, Pakistan, in 2021 and 2023, respectively, under the supervision of Dr Farooqi. Her area of research is polymer microgels and their hybrids for environmental and catalytic applications.

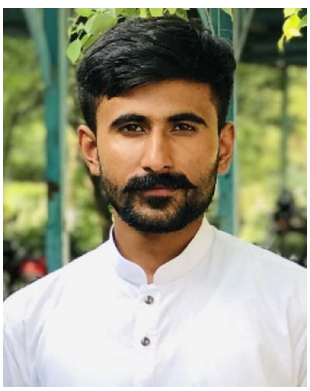

Ahmad Hassan

Ahmad Hassan obtained his BS and M. Phil degrees in Chemistry from the School of Chemistry, University of the Punjab (PU), Lahore, Pakistan, in 2021 and 2023, respectively. During his M. Phil, he worked under the supervision of Dr Farooqi. His area of research is polymer-stabilized metal nanoparticles for catalysis.

ionic strength.[25] The hybrid yolk–shell polymeric systems with an inorganic core and organic cross-linked polymeric shell have been widely reported.[26–29] A cross-linked polymeric network provides stability to inorganic particles against aggregation and imparts extra stimulus-responsive functionalities to the yolk–shell polymeric system. Moreover, the occurrence of a cavity between the core and polymeric shell provides space and protection for reactant molecules against external hindrances. Because of the mentioned fascinating features, yolk–shell hybrid microgels have been extensively used in various fields such as drug delivery,[30] selective catalysis,[17,31] nanoreactors,[22] antibacterial activities,[32] adsorption of metal ions,[26] and lithium–sulfur batteries.[33]

Because of the unique and unexplored properties of yolk–shell microgels, different approaches including distillation precipitation polymerization, free radical polymerization, reflux polymerization, etching of a silver layer, and removal of an intermediate polymeric core have been adopted for their preparation.

Robina Begum

Robina Begum is Assistant Professor at the School of Chemistry, University of the Punjab, Lahore. She obtained her PhD in Chemistry from the same institute in 2019. She carried out a part of her research work in the laboratory of Prof. Jianliang Xiao at Department of Chemistry, University of Liverpool, UK, as Split-Site PhD Scholar funded by Commonwealth Scholarship Commission, UK. Her research area is organic–inorganic hybrid materials for various applications.

Shuiqin Zhou

Shuiqin Zhou received her BS (1988) and MS (1991) degrees from Xiamen University, China, and a PhD from the Chinese University of Hong Kong in 1996. During the period 1996–2000, she worked at the State University of New York at Stony Brook as Postdoctoral Research Associate. She then worked at Union Carbide/the Dow Chemical Company as Senior Chemist until 2002 and then moved to the City University of New York at the College of Staten Island as Associate Professor. She is currently a Professor of Chemistry working in the field of microgels/nanogels, supramolecular assembly, nanomaterials, and biomaterials.

Ahmad Irfan

Dr Irfan Ahmad was graduated from GCES, University of the Punjab (PU), in 2002 and received his MSc (2004) from UAF, Faisalabad. Through a mutual scholarship of MOE, Pakistan and CSC, China, he received his PhD (2010) from NENU, China. He worked as Assistant Professor at the University of the Punjab, Lahore Pakistan and King Khalid University (KKU), Saudi Arabia. He is currently serving as Professor at Department of Chemistry and RCAMS, KKU. His present research interests are advanced functional materials, nanotechnology, catalysis, renewable energy, semiconductors, and drug designing.

Aijaz Rasool Chaudhry

Dr Aijaz Rasool Chaudhry was born in Pakistan. He completed his PhD from Universiti Teknologi Malaysia (UTM), Johor, in 2015. Currently, he is working as an Assistant Professor in the Department of Physics, College of Science, University of Bisha, Saudi Arabia. His research interests include the designing and computational modeling of new organic, inorganic, and hybrid functional materials along with the simulation and prediction of crystal structures, which are helpful in designing highly stable and efficient materials for dye-sensitized solar cells, microelectronics, and optoelectronic device applications as well as other fields of material sciences.

Zahoor H. Farooqi

Dr Zahoor H. Farooqi is currently working as Associate Professor at the School of Chemistry, University of the Punjab, Lahore, Pakistan. He worked as Research Associate in CSI, the City University of New York, USA, under Pak-US Science and Technology Cooperative Program from January 2009 to March 2010. He worked as Honorary Research Fellow in the Department of Chemistry, University of Liverpool, UK, from 01-05-2018 to 06-10-2018. He worked as a visiting Academic Staff Member in Department of Chemical Engineering, Loughborough University, UK, from 07-11-2022 to 10-01-2023. His area of research is polymer colloids and microgels loaded with inorganic nanoparticles for environmental and catalytic applications.

Many general reviews on hybrid microgels and smart microgels are available in literature.[34–37] Farooqi *et al.*[38] have described the synthesis, properties, characterization and applications of responsive microgels fabricated with gold nanostructures. Moreover, temperature-responsive hybrid microgels for catalytic applications and platinum nanoparticle fabricated multiresponsive microgel composites, along with their preparation, structural investigations, and uses have been documented by the same group.[39,40] Karg *et al.*[41] have reviewed the properties and advances in characterization of new smart poly(*N*-isopropylacrylamide) [PNIPAM] microgels and their hybrids. All the abovementioned reviews comprise all types of microgels and hybrid microgels and have been written in general. Yolk–shell microgels and yolk–shell hybrid microgels have engaged considerable interest because of their distinct and novel features. But to the extent of our knowledge, no one has reviewed the latest research achievements of these particular microgel systems.

This article describes the yolk–shell microgels and their hybrids, their classification based on their response to external stimuli, their unique properties based on the structure, different strategies used for synthesis, characterization techniques and their applications in a variety of areas.

2. Classification of yolk–shell microgels and their hybrids

Based on the responsive behavior, morphology, and nature of yolk, various yolk–shell microgels and their hybrids have been documented in previous reports.[22,28,42–45] The subsequent categorization is built upon the responsive behavior of yolk–shell microgels and their hybrids, structure, and the nature of yolk in yolk–shell microgels.

2.1 Based on responsive behavior

2.1.1 Thermoresponsive yolk–shell microgels and their hybrids. A novel class of microgels that demonstrates an immediate change in their size with a change in external temperature is called thermoresponsive microgels. For example, the yolk–shell microgels whose shell is composed of *N*-isopropylacrylamide [NIPAM] have thermo-sensitivity. At temperature lower than volume phase transition temperature (VPTT), *i.e.*, $T <$ VPTT, there is hydrogen bonding between amide groups and water molecules in the aqueous medium; thus, the PNIPAM network exists in a swollen state. The PNIPAM network gets transformed into a shrunken state[46–49] as the temperature of the medium increases above VPTT, *i.e.*, $T >$ VPTT. This feature of yolk–shell microgel system is known as thermo-sensitivity. The details of the thermo-responsive behavior of yolk–shell microgels and their hybrids are described in Section 5.1.1.

2.1.2 pH-responsive yolk–shell microgels and their hybrids. Yolk–shell microgels and their hybrids may possess functionalities like COOH and amide that can be protonated and deprotonated by varying the pH of the medium.[24,44] The microgels that can switch reversibly between the swollen and de-swollen state by changing the pH of the medium are termed as pH-responsive yolk–shell microgels. The details of pH-responsive behavior of yolk–shell microgels are discussed in Section 5.1.2.

2.1.3 Ionic strength responsive yolk–shell microgels and their hybrids. Yolk–shell microgels and their hybrids may possess ionizable functionalities in their polymeric network, which react to the variation in the ionic concentration of the medium. As a result, their size can be tuned through the change in the ionic strength of the medium.[25] Section 5.1.3 provides the details of ionic strength responsive behavior of yolk–shell microgels.

2.1.4 Multi-responsive yolk–shell microgels and their hybrids. Recently, multi-responsive yolk–shell microgels and their hybrids have attained more attention because of their potential applications in different fields.[48–51] Yolk–shell polymeric systems may contain smart polymeric core and a smart polymeric shell, and both independently respond to different stimuli. As there is no chemical interaction between the yolk and shell of the yolk–shell microgels, both can respond freely to the external stimuli. Multi-responsive yolk–shell microgels and their hybrids are widely reported in the literature.[48–50,52–54] Li *et al.*[55] have documented the preparation of narrowly dispersed poly(methacrylic acid)@void@poly(*N*-isopropylacrylamide) [PMAA@void@PNIPAM] yolk–shell polymeric microspheres with independent pH and temperature sensitivity. The independent stimuli responsive behavior was analyzed with dynamic light scattering (DLS) measurements. At an unchanging value of pH = 10, the R_h of outer polymeric shell (PNIPAM) decreased from 370 nm to 311 nm when the temperature was raised from 25 °C to 40 °C. The swelling ratio of 1.69 confirmed the temperature responsive behavior of outer PNIPAM shell. PNIPAM has VPTT of 32 °C in an aqueous medium. Below this temperature, the polymeric system is hydrophilic in nature, and water easily flows inside the shell and the size of shell is increased. When the temperature is

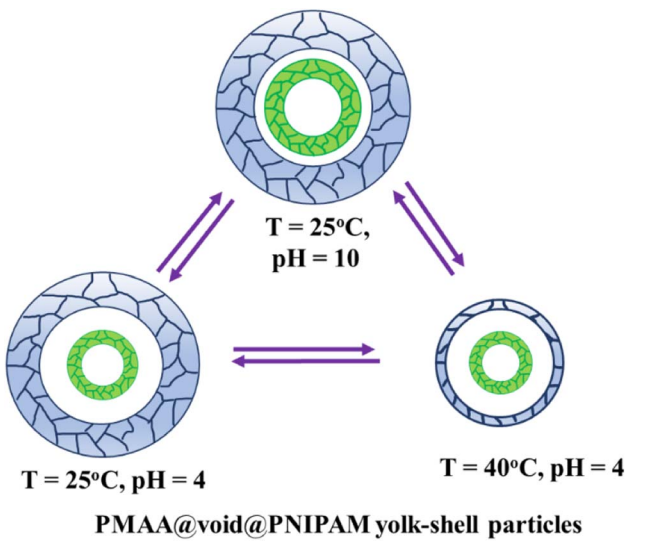

Fig. 1 Temperature and pH-responsive behavior of PMAA@void@PNIPAM yolk–shell microgels.

increased above the VPTT, the hydrophobic nature dominates, and water flow is forced to move out of the shell, decreasing the size, *i.e.*, de-swollen state. At a fixed temperature, the pH-sensitive behavior of the inner PMAA yolk is observed. The R_h changed from 160 nm to 270 nm when the pH was raised from 4 to 10. This increase in the R_h value is owing to the Donnan osmotic swelling of the PMAA shell. At higher pH values, the carboxylic acid groups of PMAA shells are completely ionized. Due to the ionization, there is an intermolecular repulsion between the carboxylic acid functionalities and the movement of water inside the shell, which increases the size of the PMAA shell. At low pH, the reverse behavior is observed. The temperature and pH-responsive behavior of the polymeric system is shown in Fig. 1.

2.2 Based on the nature of the yolk

A yolk–shell polymeric system consists of two independent structural components, *i.e.*, a yolk and a shell. The yolk can be metallic,[25,28,56,57] polymeric,[20,45,58,59] magnetic,[24,27] Au-coated Fe_3O_4,[43] silica-magnetite yolk,[24] and non-metallic (sulfur).[33] Fig. 2 represents different types of yolk–shell microgels and their hybrids based on the nature of their yolks. Following classification of yolk–shell microgels and their hybrids is based on the nature of the yolk that imparts special features to the polymeric system.

2.2.1 Yolk–shell hybrids microgel with a monometallic yolk. The yolk–shell hybrid microgels with a yolk made of single metals have attracted an expanding interest. These hybrid yolk–shell microgels have properties of both metal and polymeric network. These hybrid yolk–shell microgels exhibit excellent catalytic, chemical, and optical properties along with the responsive behavior of the polymeric network, depending upon the concentration of metal and polymeric shell. Depending upon the metallic yolk and nature of the polymeric shell, different yolk–shell hybrid microgels have been reported in the literature.[25,28,56,60] Table 1 (entries 1 to 9) shows the classification of various yolk–shell hybrid polymeric systems along with metallic yolk, characterization, and applications.

2.2.2 Yolk–shell microgels with smart polymeric yolk. Yolk–shell microgels with polymeric yolk have been widely reported in the literature.[45,58,66] A smart polymeric yolk is encapsulated in the polymeric shell, and the resulting yolk–shell microgels have features of both smart polymeric yolk and smart polymeric shell. Both the yolk and shell respond independently to the external stimuli. Table 1 (entries 10 to 17) shows the classification of yolk–shell polymeric systems having smart polymeric yolk, their classification, characterization, and application in different fields.

2.2.3 Yolk–shell hybrid microgels with magnetic yolk. Yolk–shell polymeric systems with a stable magnetic yolk have attracted the attention of modern research due to their hydrophobicity, van der Waals forces and dipole–dipole interaction, and magnetic particles' aggregates. The polymeric shell of the yolk–shell microgels provides stability and shielding against aggregation. Yolk–shell microgels with magnetic yolk used in various applications, particularly in the field of medicine, are widely reported in the literature.[27,30,67,68] Zhao *et al.*[26] reported magnetite@void@poly(methacrylic acid) [Fe_3O_4@void@PMAA] hybrid yolk–shell microspheres. Fe_3O_4 exhibits strong paramagnetic behavior. The magnetic features were investigated using a vibrating sample magnetometer (VSM) at 300 K, and the polymeric system was used for the adsorption of metal ions and drug delivery.

2.2.4 Yolk–shell hybrid microgels with Au-coated Fe_3O_4 yolk. Yang *et al.*[43] documented the fabrication of gold–magnetite@void@poly(*N*-isopropylacrylamide) [Au–Fe_3O_4@void@PNIPAM], another class of yolk–shell hybrid microgels

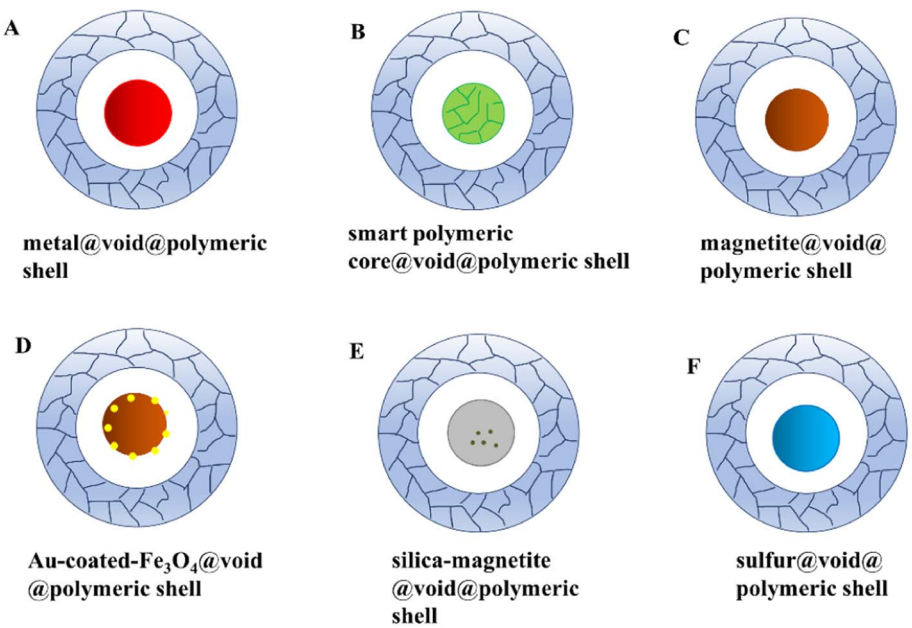

Fig. 2 Classification of yolk–shell polymeric systems on the basis of the nature of the yolk. (A) Metallic yolk, (B) smart polymeric yolk, (C) magnetite yolk, (D) Au-coated magnetite yolk, (E) silica-magnetite yolk, (F) sulfur yolk.

Table 1 Different yolk–shell polymeric systems having metallic yolk (entries 1 to 9) and polymeric yolk (entries 10 to 17); their investigation analysis and usage

S. No.	System	Yolk	Characterization techniques used	Applications	Ref.
1	Gold@void@poly(*N*-isopropylacrylamide) [Au@void@PNIPAM]	Au	TEM, DLS, UV-Vis	Tunable catalysis	17
2	Silver@void@poly(methacrylicacid) [Ag@void@PMAA]	Ag	TEM, FT-IR, EDX	Catalytic	25
3	Gold@void@poly(*N*,*N*′-methylenebisacrylamide) [Au@void@P(BIS)]	Au	TEM, XPS, UV-Vis	Nano reactors, catalytic	28
4	Gold@void@poly(*N*-isopropylacrylamide) [Au@void@PNIPAM]	Au	UV-Vis, TEM	Nanoreactor	22
5	Gold@void@microporouspolymers nanoparticles [Au@void@MPNPs]	Au	TEM, DLS, XRD, UV-Vis	Antibacterial, catalytic	32
6	Palladium@void@poly-4-vinylbenzylchloride-*g*-poly (acrylamide) [Pd@void@P(CMSt-*g*-PAA)]	Pd	TEM, SEM, FT-IR, XPS, ICP, TGA, DLS, UV-Vis	Catalytic	56
7	Gold@void@poly(benzyl methacrylate) [Au@void@PBzMA]	Au	SEM, TEM, UV-Vis		60
8	Ruthenium@void@polystyrene [Ru@void@PS]	Ru	TEM, XRD, XPS	Catalysis	61
9	Platinum@void@poly (cyclotriphosphazene-*co*-4,4′-sulfonyldiphenol) [Pt@void@PZS]	Pt	TEM, FESEM, UV-Vis, XPS, FT-IR	Catalysis	62
10	Poly(methacrylic acid-*co*-ethyleneglycol dimethacrylate)@void@poly (*N*-isopropylacrylamide-*co*-methacrylic acid) [P(MAA-*co*-EGDMA) @void@P(NIPAM-*co*-MAA)]	P(MAA-*co*-EGDMA)	FT-IR, TGA, TEM, DLS	Drug delivery	23
11	Polymethacrylic acid@void@poly(*N*-isopropylacrylamide) [PMAA@void@PNIPAM]	PMAA	TEM, FT-IR, DLS	Drug delivery	63
12	Poly(2-(diethylamino)ethyl methacrylate-styrene)@void@polystyrene [PDS@void@PS]	PDS	TEM, FT-IR, DLS, UV-Vis	Drug delivery	64
13	Cross-linked polymethacrylic acid@void@cross-linked poly(*N*-isopropylacrylamide) [CPMAA@void@CPNIPAM]	CPMAA	TEM, FT-IR, DLS, UV-Vis	Drug delivery	59
14	Poly(acrylic acid)@void@poly(2-hydroxyethyl methacrylate) [PAA@void@PHEMA]	PAA	TEM, FESEM, FT-IR	Drug delivery	65
15	Poly(divinylbenzene-*co*-acrylic acid) @void@poly(divinylbenzene-*co*-acrylic acid) [P(DVB-*co*-AA)@void@P(DVB-*co*-AA)]	P(DVB-*co*-AA)	TEM, FT-IR, DLS	Drug delivery	45
16	Polymethacrylic acid@void@poly(*N*-isopropylacrylamide) [PMAA@void@PNIPAM]	PMAA	CLSM, FT-IR, TEM, FESEM	Drug delivery	55
17	Poly(methacrylic acid-*co*-ethyleneglycol dimethacrylate)@void@poly(*N*-isopropylacrylamide) [P(MAA-*co*-EGDMA) @void@PNIPAM]	P(MAA-*co*-EGDMA)	FT-IR, TGA, DLS, TEM	Drug delivery	42

with Au-coated Fe_3O_4 yolk and the thermo-responsive PNIPAM shell. Because of the magnetic properties of the magnetite yolk, it can hold gold nanoparticles (Au NPs) and can be isolated from the reaction mixture using a simple magnet. The simultaneous hydrolysis of 3-aminopropyl triethylsilane (APTES) and tetraethyl orthosilicate (TEOS) modified the surface of magnetite (Fe_3O_4) with amino groups and Au NPs attracted to the Fe_3O_4 surface by self-assembly (an autonomous process driven by mutual interactive forces to arrange disordered particles into a well-organized pattern). The prepared hybrid polymeric system was characterized by FT-IR and VSM, and it showed excellent catalytic properties and recyclability.

2.2.5 Yolk–shell hybrid microgels with silica-magnetite yolk. Fe_3O_4 particles have a vast variety of applications, but

owing to the inter-particle interactions, Fe_3O_4 particles aggregate, which limits their usage. Liu *et al.*[24] have described the fabrication of silica-magnetite@void@poly(*N*,*N*′-methylenebisacrylamide-*co*-methacrylic acid) [SiO_2–Fe_3O_4@void@P(BIS-*co*-MAA)] yolk–shell hybrid polymeric system with silica-magnetite yolk and pH-responsive shell. Fe_3O_4 particles were coated with SiO_2 to enhance their stability and properties. First, SiO_2 provides shielding against the inter-particle interaction of Fe_3O_4; secondly, a large number of silanol groups on the SiO_2 surface endows magnetite particles with functionalities. The Fe_3O_4 properties of the prepared yolk–shell hybrid microgels were investigated by VSM at room temperature. Owing to the pH-responsive behavior of the polymeric shell, SiO_2–Fe_3O_4@void@P(BIS-*co*-MAA) finds application in targeted drug delivery systems. The size of the [SiO_2–Fe_3O_4@void@P(BIS-*co*-MAA)] yolk–shell hybrid polymeric system was determined using TEM and found to be 114 nm.

2.2.6 Yolk–shell hybrid microgels with sulfur yolk. Zhang *et al.*[33] reported sulfur@void@polypyrrole [S@void@PPy] yolk–shell hybrid microgels having sulfur as a yolk. The structure and morphology of the prepared S@void@PPy polymeric system was investigated and proved by XRD, XPS, FT-IR, RS and SEM analysis. The polymeric shell (PPy) has conductive properties. These polymeric systems can be effectively used in lithium–sulfur batteries. This new class of yolk–shell hybrid microgels has a stable porous structure and empty space between the core and shell region, which help in the volume changes of sulfur during the charging and discharging cycles of batteries. The detail is discussed in Section 6.5 of the article.

2.3 Based on morphology

Different morphologies of yolk–shell microgels and their hybrids induce special features into their structures and enhance their applications in various fields. Yolk–shell polymeric systems may have raspberry-shaped structure,[59] elliptical,[29] lemon like morphology,[69] double shell,[44,68] and rattles like structures,[70] as shown in Fig. 3.

The following classification of yolk–shell polymeric systems and their hybrids is based on their morphology.

2.3.1 Raspberry-shaped yolk–shell microspheres. Liu *et al.*[59] have explored the fabrication of raspberry-shaped cross-linked poly(methacrylicacid)@poly(*N*-isopropylacrylamide) [RS-CPMAA@CPNIPAM] system having independent pH and temperature response *via* the self-removal process. The prepared yolk–shell polymeric system was characterized by TEM, DLS, FT-IR, and UV-Vis analysis. TEM images asserted that the prepared polymeric system was different from general yolk–shell morphology; rather, it possesses raspberry-shaped morphology (with diameter of 116.3 nm). The strong hydrogen bonding between the amide groups of PNIPAM and carboxylic acid functionalities of PMAA affected the general yolk–shell morphology. Moreover, a higher concentration of NIPAM in the outer shell might be the reason for this morphology. The RS-CPMAA@CPNIPAM polymeric system showed an excellent and fast response to the variation in pH and temperature of the medium.

2.3.2 Elliptical yolk–shell microgels. Hao *et al.*[29] have documented the preparation of hematite@void@polypyrrole [Fe_2O_3@void@PPy] yolk–shell polymeric system by the selective elimination of the SiO_2 layer from [Fe_2O_3@SiO_2@PPy] by hydrofluoric acid (HF). This polymeric system has a hematite olivary particles (α-Fe_2O_3) as a moveable yolk inside the polypyrrole (PPy) as an external cross-linked shell, as confirmed by the TEM images. The anisotropic moveable yolk inside the polymeric network finds different potential applications in biological delivery systems.

2.3.3 Lemon-like structures. Gua *et al.*[69] have reported the preparation of polymer-based yolk–shell microgels with tunable morphologies. The polymeric shell of poly(2-vinyl-4,4-dimethylazlactone) (PVDMA) was synthesized on the SiO_2 layer, which was removed through HF, and a hollow polymeric

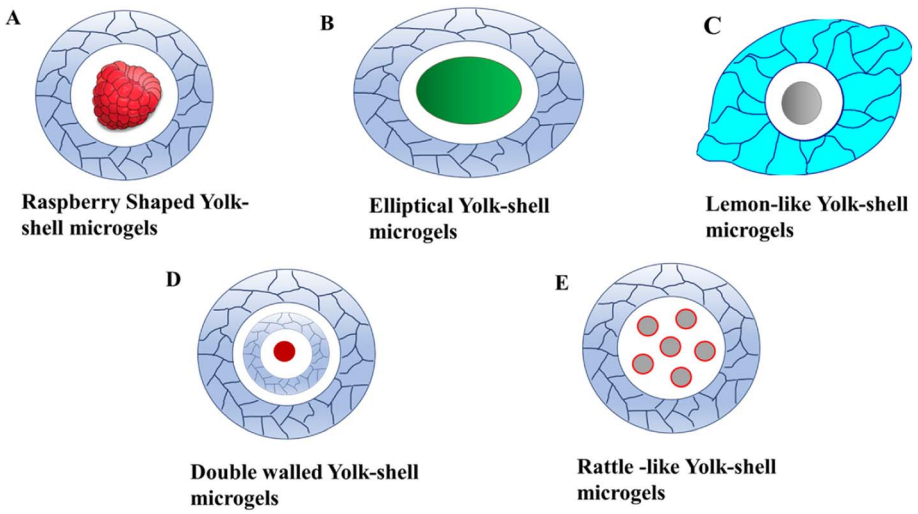

Fig. 3 Yolk–shell microgels with different morphologies: (A) raspberry-shaped, (B) elliptical, (C) lemon-like morphology, (D) double walled, (E) rattle-like morphology.

network with functionalized tertiary amine groups was obtained. Using a model isotropic oil, tetradecane was infused into the hollow polymeric network by the extraction of oil-filled capsules using deionized water. The emerged microgel was a yolk–shell polymeric system with lemon like polymeric shell. This lemon like morphology was proved by bright field microscopy, fluorescence microscopy and SEM analysis and size was found to be 11.3 ± 0.6 μm.

2.3.4 Double-walled yolk–shell polymeric system. Double-walled yolk–shell polymeric systems like silica@void@poly(-methacrylic acid)@void@poly(*N*-isopropylacrylamide) [Fe_3O_4@void@PMAA@void@PNIPAM] with pH-responsive and temperature responsive behavior have been reported in the literature.[68] The magnetic yolk imparts magnetic properties to the polymeric system. First, Fe_3O_4@SiO_2@PMAA@SiO_2@-PNIPAM five-layered core–shell microspheres with onion shape were prepared by precipitation polymerization following the etching of both SiO_2 layer with HF. The resulting polymeric system [Fe_3O_4@void@PMAA@void@PNIPAM] has a magnetic yolk, inner cross-linked PMAA shell with pH-sensitive behavior and an outer cross-linked PNIPAM shell with thermo-sensitive behavior.

2.3.5 Rattle-like yolk–shell microgels. Zou *et al.*[70] reported the synthesis of the rattle-like polymeric system by oil-in-water (O/W) pickering emulsion polymerization. The hydrophobic SiO_2 particles were dispersed in oil phase containing styrene (St), hexadecane (HD), and divinyl benzene (DVB). Lignin nanoparticles were added as the pickering agent, which produced O/W emulsion, followed by the polymerization of monomers (St and DVB) to produce polymeric shell (P(St-DVB)) having rattle-like cores. Increasing the concentration of the pickering agent increases the number of cores and decreases the size of the polymeric shell, while increasing the HD concentration reduces the number of cores and a single solid core is formed. The prepared polymeric system was characterized using energy dispersive scattering (EDS) and FT-IR analysis to confirm the formation of rattle-like yolks surrounded by a polymeric network.

3. Synthesis strategies used

Yolk–shell microgels and their hybrids can be prepared using various methodologies. Some of the preparation methods are illustrated in detail as given below.

3.1 By the removal of poly(methacrylic acid) layer

The preparation of pH-responsive hollow poly(*N*,*N*′-methylenebisacrylamide-*co*-methacrylic acid) [P(BIS-*co*-MAA)] microspheres with moveable magnetic/silica (Fe_3O_4/SiO_2) core *via* the selective elimination of poly(methacrylic acid) [(PMAA)] layer in ethanol/water from Fe_3O_4/SiO_2/PMAA/P(BIS-*co*-MAA) four-layered microspheres has been reported in the literature.[71] Magnetite (Fe_3O_4) nanoparticles (NPs) were synthesized through the chemical co-precipitation of Fe^{2+} and Fe^{3+} under alkaline conditions *via* the sol–gel process. In the next step, Fe_3O_4/SiO_2 core–shell particles were fabricated by the Stöber

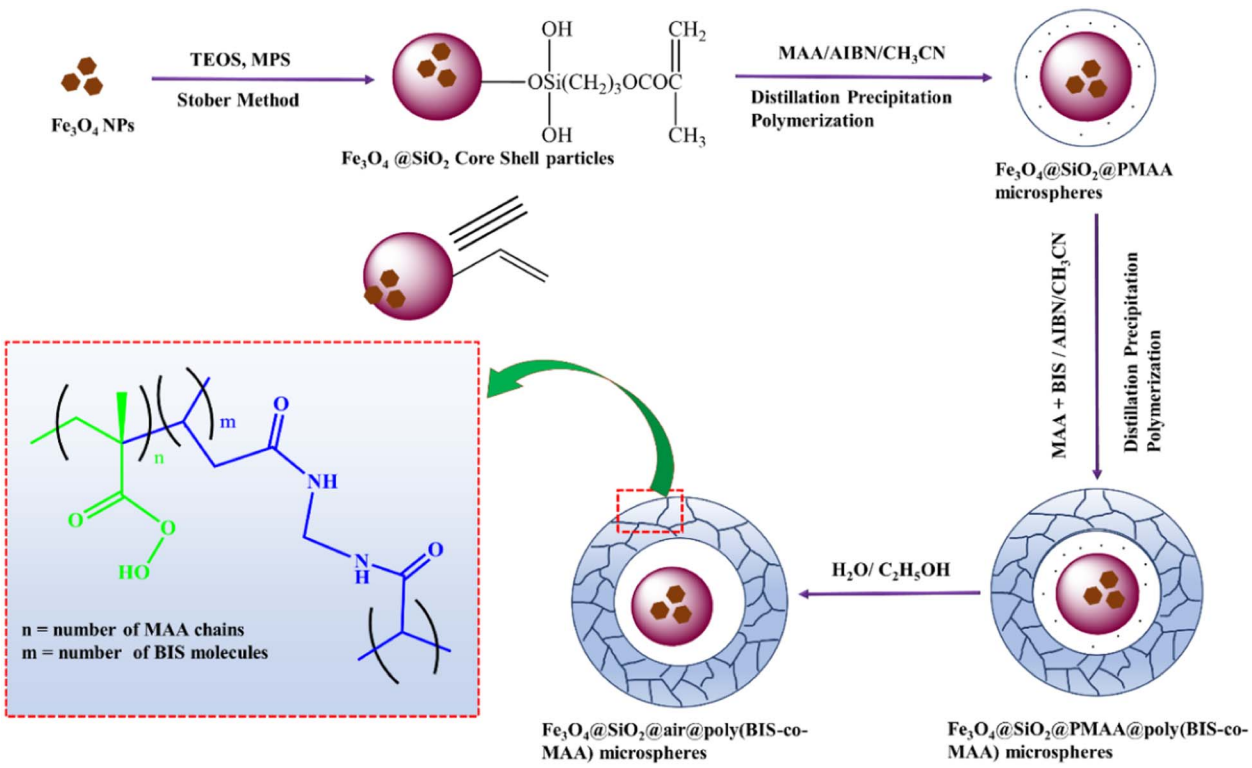

Fig. 4 Fabrication of Fe_3O_4/SiO_2/air/P(BIS-*co*-MAA) yolk–shell microspheres from Fe_3O_4/SiO_2/PMAA/P(BIS-*co*-MAA) tetra-layer microspheres by the removal of non-crosslinked poly(methacrylic acid) layer using ethanol.

process and modified by employing 3-(methacryloxy)propyl trimethoxysilane (MPS). Then, these MPS-modified Fe_3O_4/SiO_2 NPs were dispersed in acetonitrile to be used as the seed to fabricate three-layered Fe_3O_4/SiO_2/PMAA microspheres *via* distillation precipitation polymerization with the addition of methacrylic acid (MAA) as a monomer and 2,2′-azobisisobutyronitrile (AIBN) as the initiator during the polymerization process, thus generating three-layered Fe_3O_4/SiO_2/PMAA microspheres, as illustrated in Fig. 4. Then, Fe_3O_4/SiO_2/PMAA/P(BIS-*co*-MAA) four-layered microspheres were prepared by distillation precipitation polymerization, where Fe_3O_4/SiO_2/PMAA three-layered microspheres were used as seeds with the addition of MAA as the monomer, *N*,*N*′-methylenebisacrylamide (BIS) as the cross-linker and AIBN as the initiator during polymerization. Then, from the resultant Fe_3O_4/SiO_2/PMAA/P(BIS-*co*-MAA) four-layered microspheres, the non-crosslinked PMAA middle layer was selectively eliminated with the help of ethanol/water (EtOH/H_2O) solvent. Thus, the resulting structure was Fe_3O_4/SiO_2/air/P(BIS-*co*-MAA) microspheres.

3.2 By the self-removal process

Yolk–shell microgel particles can be synthesized *via* the "self-removal process". Raspberry-shaped cross-linked poly(methacrylic acid)@cross-linked poly(*N*-isopropylacrylamide) [CPMAA@CPNIPAM] yolk–shell microspheres have been prepared using this method.[72] For this purpose, CPMAA nanoparticles were prepared *via* distillation polymerization using methacrylic acid (MAA) as the monomer, AIBN as the initiator and ethylene glycol dimethacrylate (EGDMA) as the cross-linker, as shown in Fig. 5.

Then, CPMAA@PNIPAM@CPNIPAM microsphere particles were fabricated by seeded emulsion polymerization using CPMAA, NIPAM, sodium dodecyl sulfate (SDS) as the surfactant and ammonium persulfate (APS) as the initiator during the process, thus generating CPMAA@PNIPAM microsphere particles. Then, at the end of polymerization, cross-linker, divinyl benzene (DVB), monomer (NIPAM) and APS (initiator) were supplemented again into the mixture. The reaction was carried out for 4 hours at 70 °C and allowed to settle at room temperature for the "self-removal process". This decrease in temperature caused non-cross-linked PNIPAM globules to be changed into a coil-type structure. In this way, the mid-layer of CPMAA@PNIPAM@CPNIPAM was removed to obtain CPMAA@CPNIPAM yolk–shell microspheres.

3.3 *Via* free radical polymerization

Free radical polymerization has various advantages of quickness and simplicity in synthesis as well as the need of sophisticated and costly instrumentation is also avoided. Wu *et al.*[47] have documented the preparation of thermo-sensitive, gold-poly(*N*-isopropylacrylamide) [Au-PNIPAM] yolk–shell particles *via* free radical precipitation polymerization. For this purpose, first of all, Au–SiO_2 was modified by sodium silicate (SS). [Au–SiO_2-SS] core–shell nanoparticles were prepared. 3-Aminopropyl trimethosysilane (APM) was added to Au sol prepared by sodium citrate reduction process with fifteen minutes of magnetic stirring. Then, to this surface modified Au sol, active SiO_2 was added, the solution was stirred and after 24 hours, ethanol, tetraethyl orthosilicate (TEOS) and ammonia (NH_3) were introduced into mixture. The reaction mixture was left undisturbed for 2 days with magnetic stirring and then SiO_2

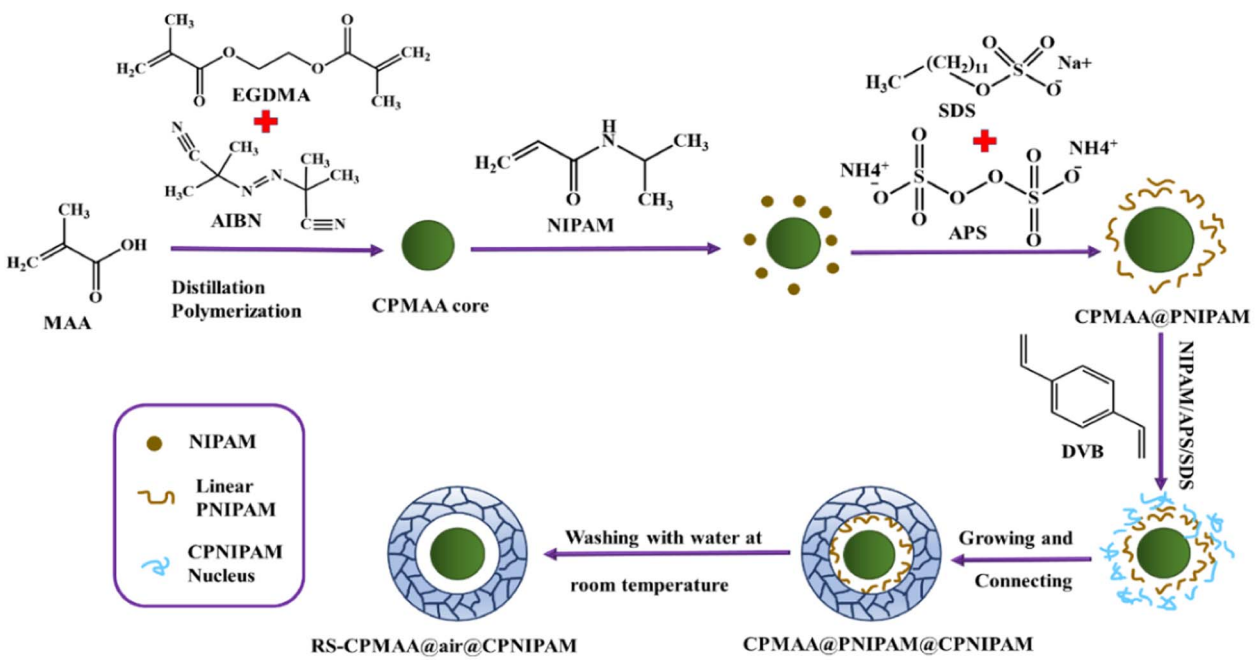

Fig. 5 Synthesis of raspberry-shaped cross-linked poly(methacrylic acid)@cross-linked poly(*N*-isopropylacrylamide) [CPMAA@CPNIPAM] yolk–shell microspheres from CPMAA@PNIPAM@CPNIPAM by the self-removal of non-cross-linked PNIPAM.

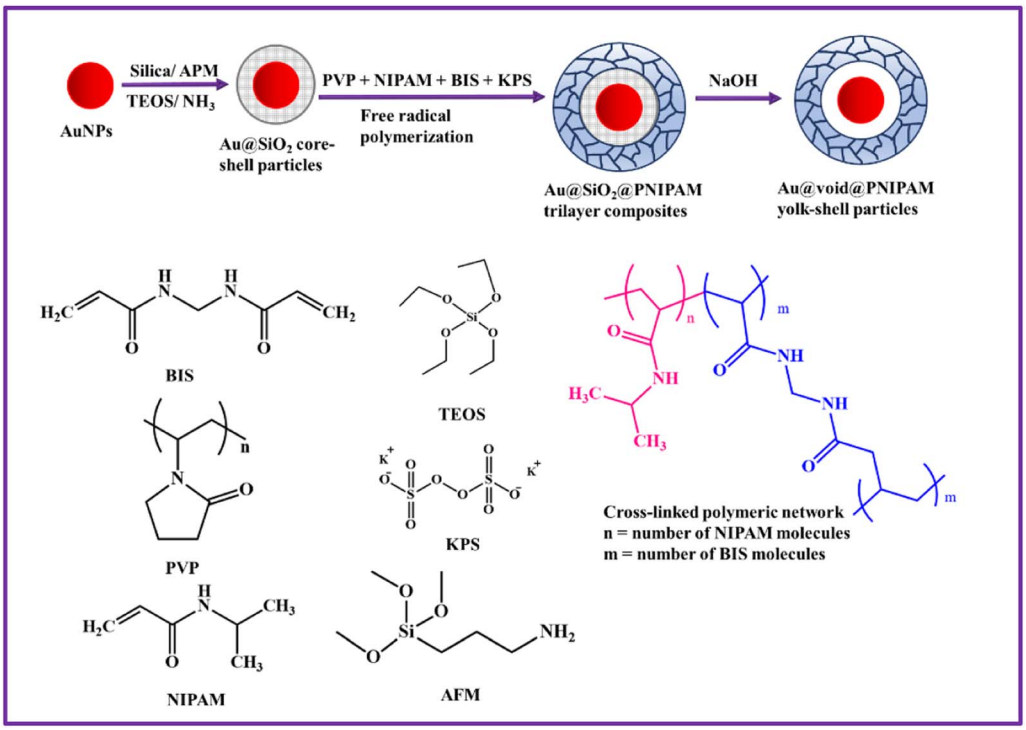

Fig. 6 Synthesis of gold–poly(*N*-isopropylacrylamide) [Au–PNIPAM] yolk shell particles *via* free radical polymerization.

surface was modified using SS, thus generating Au–SiO_2-SS core–shell nanoparticles. Then, Au–SiO_2-PNIPAM tri-layer composites were prepared using Au–SiO_2 core–shell particles as seeds using conventional radical polymerization, as shown in Fig. 6.

The Au–SiO_2 core–shell particles in ethanol solution were dispersed into poly(vinylpyrrolidone) (PVP) stabilizer. After 15 minutes, NIPAM and BIS were added into the reaction mixture. The reaction proceeded in the presence of nitrogen atmosphere and with the addition of potassium per sulfate (KPS) as the initiator, the polymerization was started and the polymerization process lasted for 4 hours at 70 °C, thus fabricating the Au–SiO_2-PNIPAM tri-layer composites. Then, the Au-PNIPAM yolk–shell particles were prepared from Au–SiO_2-PNIPAM tri-layer composites by the etching of the middle layer, *i.e.*, SiO_2 by dissolution in sodium hydroxide (NaOH).

But this method has some disadvantages as, for example, during the free radical polymerization process, it is not easy to monitor the rate of chain propagation; thus, there will be broad-sized particles. To overpower this drawback, reversible addition–fragmentation chain transfer (RAFT) polymerization is used to synthesize yolk–shell microgels.

3.4 *Via* reversible addition–fragmentation chain transfer polymerization

Reversible addition–fragmentation chain transfer (RAFT) polymerization is a kind of living polymerization concerning a conventional radical polymerization that is facilitated *via* a RAFT agent. RAFT is termed as living or controlled radical polymerization[73] and has the advantage that the nanoparticles cores can be formed *in situ* using this method; the polymerization process occurs in moderate polymerization conditions and a vast variety of functional monomers can be used in this method. Xu *et al.*[61] documented the formation of yolk–shell structured hollow porous polymeric nanospheres *via* RAFT polymerization. For this purpose, a mixture of styrene as a monomer, modified polylactide macrochain transfer agent (PLA-CTA) whose CTA functional groups acted as the RAFT groups for chain extension, AIBN as the initiator was added to the vessel to carry out RAFT polymerization at 70 °C for 24 hours, thus generating the polylactide-*b*-polystyrene diblock copolymer (PLA-*b*-PS). Then, the dissolution of reaction mixture was carried in carbon tetrachloride (CCl_4) solution along with ferric chloride ($FeCl_3$) as a catalyst. $FeCl_3$ was used here as a Lewis acid (triggers Friedel–Crafts alkylation reaction), thus resulting in the hyper cross-linking of polystyrene, as shown in Fig. 7(A). Moreover, the hyper cross-linking-directed self-assembly of PLA-*b*-PS diblock copolymer precursors into the core–shell microsphere structure also took place. Then, after one day at 90 °C, ethanol and water solution was introduced into the reaction mixture for the termination of the reaction. Moreover, the hollow cavity in the polymeric framework was created by the degradation of PLA with the help of byproducts of Friedel–Craft reaction, *i.e.*, hydrochloric acid (HCl) and $FeCl_3$, resulting in the fabrication of hollow porous polymeric nanospheres. Finally, to encapsulate Pd nanoparticles, the hollow porous polymeric nanospheres were dispersed in dimethylformamide (DMF). Palladium(II) acetate [$Pd(OAc)_2$] dissolved in DMF was mixed dropwise to the reaction mixture and agitated for 24 hours at room temperature. The resulting

powder was separated by centrifugation, dispersed in DMF and, ultimately, sodium borohydride as the reducing agent was added to the reaction mixture, resulting in the formation of palladium (Pd) nanoparticles inside the yolk–shell-structured hollow porous polymeric nanospheres. Then, the same group also reported the metal ions of ruthenium (Ru) and platinum (Pt) addition into the same yolk–shell-structured hollow porous polymeric microspheres, followed by reduction with $NaBH_4$. The whole process is shown in Fig. 7(B).

However, the drawback of this method is that the polymeric shell coated on inorganic yolk by the RAFT polymerization process leads to a thin coating of the shell and there is also difficulty in the post-treatment of the product owing to the used RAFT reagent. Distillation precipitation polymerization is used to overcome this drawback.

3.5 *Via* distillation precipitation polymerization

The most widely used surfactant-free heterogeneous polymerization process for the fabrication of hollow nanostructures with uniform shape is distillation precipitation polymerization.[74] It is the most impactful strategy for covering hydrophilic polymer on inorganic particles. The distillation precipitation polymerization strategy for the fabrication of yolk–shell microgel particles is one of the most widely reported methods in the

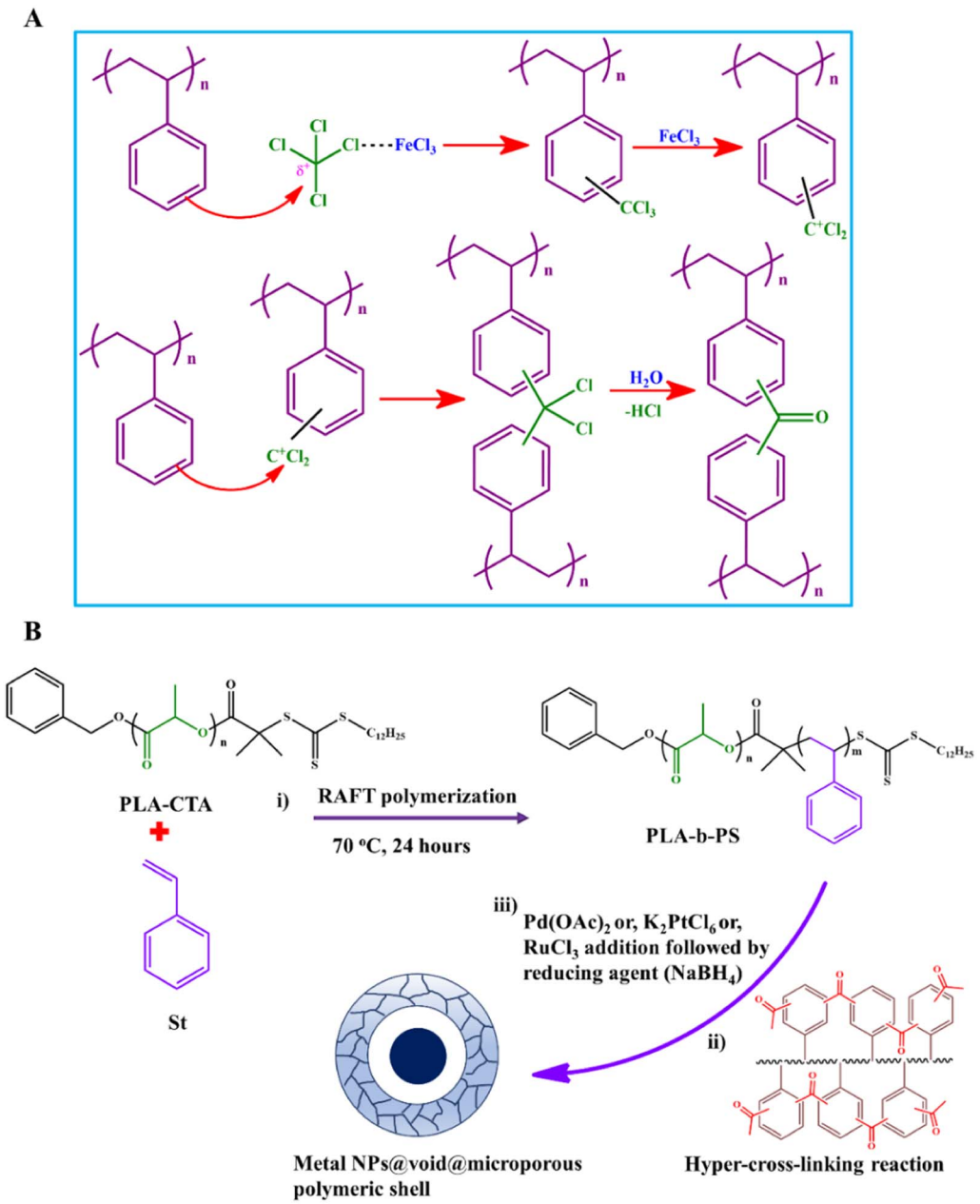

Fig. 7 (A) $FeCl_3$-triggered Friedel–Crafts reaction for the cross-linking of polystyrene. (B) Synthesis of hollow porous polymeric nanospheres having metallic yolk *via* RAFT polymerization.

literature.[48,49,52,53,74–76] Du *et al.*[49] explored the preparation of poly(methacrylic acid-*co*-ethyleneglycol dimethacrylate)@poly(*N*-isopropylacrylamide) [P(MAA-*co*-EGDMA)@PNIPAM] yolk–shell microspheres *via* the distillation precipitation polymerization method. For this purpose, first of all, poly(-methacrylic acid-*co*-ethyleneglycoldimethacrylate) [P(MAA-*co*-EGDMA)] microgels cores were fabricated using facile distillation precipitation copolymerization of MAA and EGDMA with AIBN as the initiator in acetonitrile. Then, an outer SiO_2 layer was coated onto the P(MAA-*co*-EGDMA) microgels cores by the sol–gel process to fabricate the poly(methacrylic acid-*co*-ethyleneglycol dimethacrylate)@silica [(P(MAA-*co*-EGDMA)@SiO_2] core–shell microspheres. For this purpose, the P(MAA-*co*-EGDMA) microgels cores, ammonia and tetraethyl orthosilicate (TEOS) were incorporated to H_2O–ethanol mixture under stirring, the sol–gel process proceeded for 12 hours and then the P(MAA-*co*-EGDMA)@SiO_2 core@shell microgel particles were modified using MPS to introduce reactive vinyl groups. Then, these MPS-modified P(MAA-*co*-EGDMA)@SiO_2 core@shell microgel particles were used as seeds to synthesize poly(-methacrylicacid-*co*-ethyleneglycoldimethacrylate)@silica@poly(*N*-isopropylacrylamide) [(P(MAA-*co*-EGDMA)@SiO_2@PNIPAM] three-layered sandwich microspheres *via* the distillation precipitation copolymerization of BIS and NIPAM as the monomer and AIBN as the initiator in acetonitrile. Then, the prepared [P(MAA-*co*-EGDMA)@SiO_2@PNIPAM] microspheres were drowned in hydrofluoric acid (HF), which caused the etching of the SiO_2 layer, resulting in PMAA-*co*-EGDMA@PNIPAM yolk–shell microspheres, as illustrated in Fig. 8.

However, in distillation precipitation polymerization, a desirable production rate cannot be attained. Moreover, acetonitrile as the solvent is very toxic, adding to the disadvantages of distillation precipitation polymerization. This is the drawback of distillation precipitation polymerization method, which can be overcome using the seed emulsion polymerization technique for the preparation of yolk–shell microgels.

3.6 *Via* seed emulsion polymerization

The fabrication of yolk–shell microspheres *via* the seed emulsion polymerization method has been listed in the literature.[26,58] Zhao *et al.*[26] have reported the fabrication of yolk–shell magnetite@void@poly(methacrylic acid) [Fe_3O_4@void@PMAA] composite microspheres using seeded emulsion polymerization. For this purpose, first of all, super-paramagnetic Fe_3O_4 particles were fabricated by the solvothermal method; iron(III) chloride hexahydrate ($FeCl_3 \cdot 6H_2O$), trisodium citrate and sodium acetate were dissolved in ethylene glycol (EG) and diethylene glycol (DEG) under stirring for 30 minutes; the mixture was autoclaved and heated for 10 hours at 200 °C and cooled at room temperature to finally obtain super-paramagnetic Fe_3O_4 particles. To prepare magnetite@silica (Fe_3O_4@SiO_2) composite microspheres, the SiO_2 shell was fabricated employing the Stöber method. The Fe_3O_4 particles were dispersed in ethanol, water and ammonia, and the mixture was ultra-sonicated. Then, TEOS was mixed into the reaction mixture, and the solution was stirred for 6 hours at 30 °C to finally obtain Fe_3O_4@SiO_2 composite microspheres. The surface of Fe_3O_4@SiO_2 composite microspheres was modified by dispersing them into ethanol, and MPS is added into the dispersion for the introduction of vinyl groups to get the modified Fe_3O_4@SiO_2-MPS composite microspheres. Then, the core–shell–shell Fe_3O_4@SiO_2@PMAA composite microspheres were prepared by seeded emulsion polymerization, as shown in Fig. 9.

For this purpose, the Fe_3O_4@SiO_2-MPS composite microspheres dispersed in ethanol are mixed with SDS *via* mechanical

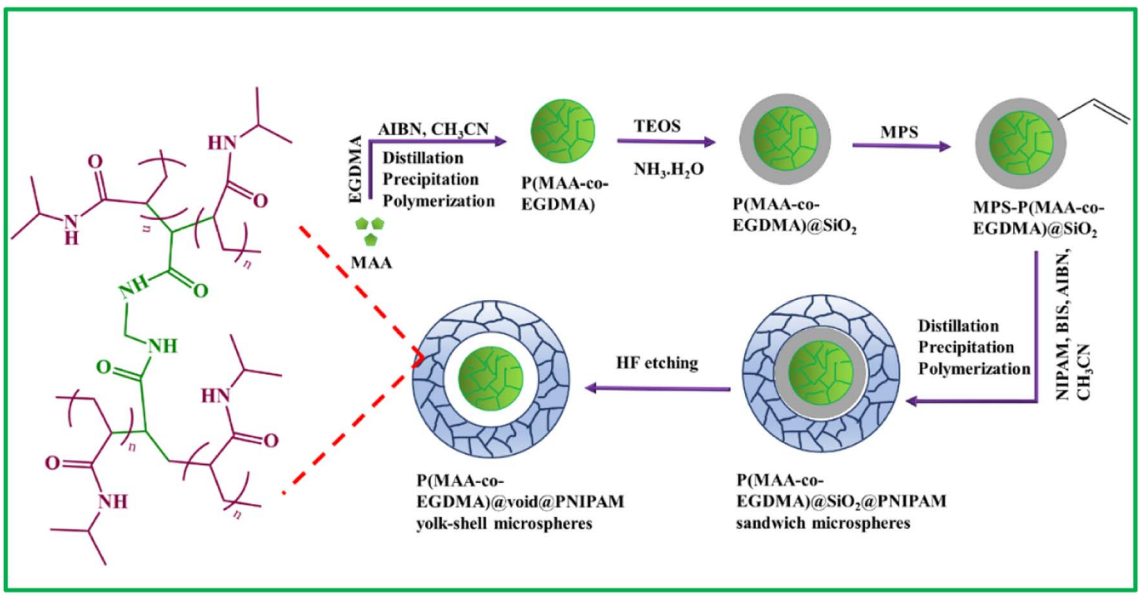

Fig. 8 Synthesis of poly(methacrylic acid-*co*-ethyleneglycoldimethacrylate)@poly(*N*-isopropylacrylamide) [(PMAA-*co*-EGDMA)@PNIPAM] yolk–shell microspheres *via* the distillation precipitation polymerization method.

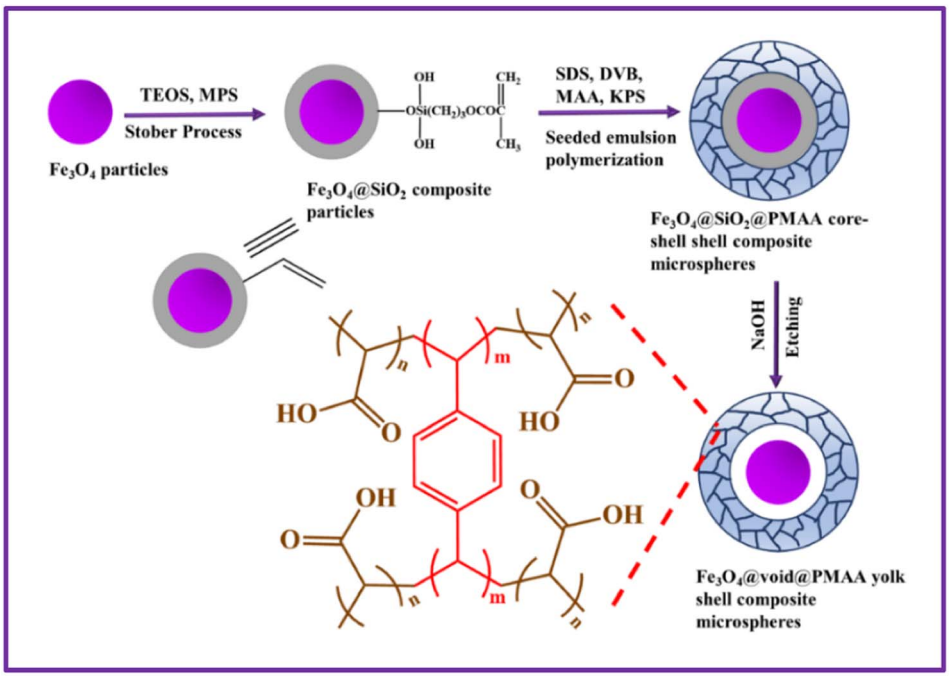

Fig. 9 Fabrication of yolk–shell magnetite@poly(methacrylic acid) [(Fe_3O_4@PMAA)] composite microspheres using seeded emulsion polymerization.

stirring. Degassing was done with nitrogen, after which cross-linker DVB and monomer MAA were introduced into the reaction mixture and heated at 70 °C. Then, the initiator KPS was added to the dispersion to initiate polymerization; the reaction proceeded for 7 hours to obtain Fe_3O_4@SiO_2@PMAA composite microspheres. The yolk–shell Fe_3O_4@PMAA composite microspheres were prepared by etching the middle layer of Fe_3O_4@SiO_2@PMAA composite microspheres with the help of NaOH.

3.7 *Via* reflux-precipitation polymerization

The advantage of using reflux precipitation polymerization technique for the preparation of yolk–shell microgels is that it is carried out as a continuous or batch process. This feature helps to get yolk–shell microgel particles with desired properties. This process allows control over properties like size distribution, chemical composition and surface charge. Yang *et al.*[30] reported the formation of magnetite@void@poly(methacrylic acid) [Fe_3O_4@void@PMAA] yolk–shell microspheres by reflux-precipitation polymerization method. For this purpose, first of all, poly(γ-glutamic acid) (PGA)-modified Fe_3O_4 nano-clusters were prepared using the solvothermal reaction. Iron(III) chloride hexahydrate ($FeCl_3 \cdot 6H_2O$), PGA (as stabilizer) and ammonium acetate (NH_4OAc) were immersed in ethylene glycol, the mixture was supplied with nitrogen atmosphere with stirring for 1 hour at 160 °C and then transferred to an autoclave, whereby it was heated at 200 °C for fifteen hours and left to cool at room temperature to obtain PGA-modified Fe_3O_4 nano-clusters. These PGA-modified Fe_3O_4 nano-clusters were then used to fabricate core/shell magnetite@uncross-linked poly(-methacrylic acid) (Fe_3O_4@u-PMAA) microspheres using the reflux-precipitation polymerization, as shown in Fig. 10.

PGA-modified Fe_3O_4 nano-clusters, MAA and AIBN were dissolved in acetonitrile (AN); the reaction mixture was ultrasonicated and heated at 110 °C for 3 hours to fabricate

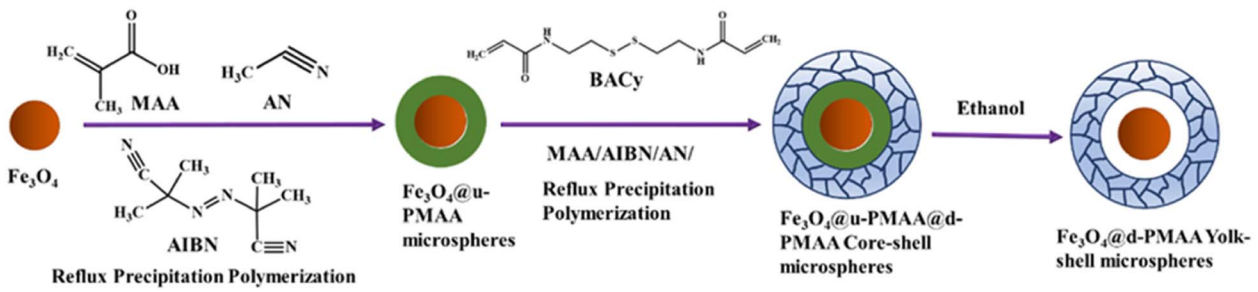

Fig. 10 Synthesis of magnetite@poly(methacrylic acid) [Fe_3O_4@PMAA] yolk–shell microspheres *via* the reflux-precipitation polymerization method.

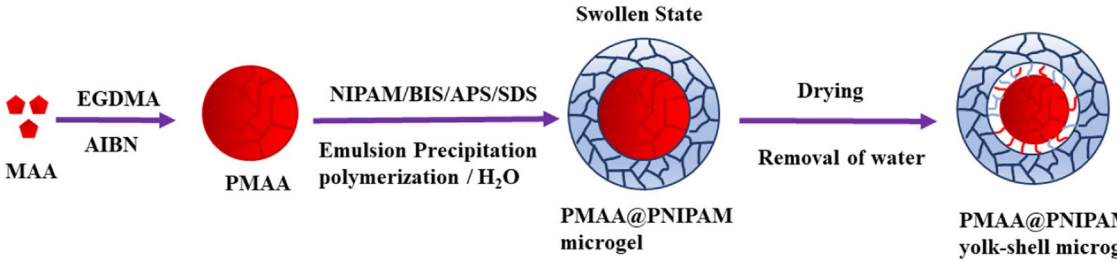

Fig. 11 Synthesis of poly(methacrylic)@void@poly(*N*-isopropropyl-acrylamide) [PMAA@void@PNIPAM] yolk–shell microgels through emulsion precipitation polymerization.

Fe_3O_4@u-PMAA microspheres. Then, these Fe_3O_4@u-PMAA microspheres were immersed in AN as seeds to fabricate disulfide cross-linked poly(methacrylic acid) (d-PMAA)-coated Fe_3O_4@u-PMAA@d-PMAA core–shell microspheres employing reflux precipitation polymerization. To synthesize Fe_3O_4@u-PMAA@d-PMAA core–shell microspheres, Fe_3O_4@u-PMAA, *N*,*N*-bis(acryloyl)cystamine (BACy) as cross-linker, AIBN and MAA were dissolved in AN. Then, finally, the Fe_3O_4@u-PMAA@d-PMAA core–shell microspheres were immersed in ethanol for three hours to remove the uncross-linked PMAA cores to obtain yolk–shell Fe_3O_4@PMAA microspheres.

The limitation of reflux precipitation polymerization method is that due to high polymerization temperature, only the thermo-stable material can be used. This drawback can be overcome using the emulsion precipitation polymerization method for the synthesis of yolk–shell microgels.

3.8 *Via* emulsion precipitation polymerization

Liu *et al.*[50] documented the synthesis of pH and temperature dual-responsive poly(methacrylic)@void@poly(*N*-isopropropyl-acrylamide) [PMAA@void@PNIPAM] yolk–shell microgels having pH-responsive PMAA cores and temperature-sensitive PNIPAM shells using emulsion precipitation polymerization. For this purpose, first of all, the PMAA cores were fabricated *via* distillation precipitation polymerization by dissolving MAA, cross-linker ethylene glycol dimethacrylate (EGDMA) and initiator (AIBN) into acetonitrile. Then, a facile emulsion precipitation polymerization method was used to fabricate PMAA@void@PNIPAM yolk–shell microgels. PMAA cores, NIPAM, BIS and sodium dodecyl sulfate (SDS) were dispersed into water, as shown in Fig. 11.

The reaction mixture was heated to 70 °C after degassing with nitrogen and ammonium persulfate (APS) was added as an initiator to carry out the polymerization process for 6 hours, thus fabricating the PMAA@PNIPAM microgels. All the core and shell materials in PMAA@PNIPAM microgels shrank by removing the solvent (H_2O). Due to full swelling in H_2O, the PMAA cores in the PMAA@PNIPAM microgels showed greater volume shrinkage ratio, which resulted in the formation of a hollow layer between the PNIPAM shells and PMAA cores, thus fabricating PMAA@void@PNIPAM yolk–shell microgels. But Liu *et al.*[50] were not able to give intuitive proof for the yolk–shell structure of PMAA@void@PNIPAM microgels. The drawback of this strategy is that the encapsulation efficiency of polymeric shell on the yolk was low for emulsion precipitation polymerization.

4. Characterization

To discover morphology and structural changes due to the external stimuli of yolk–shell microgels and their hybrids, various analytical techniques are used. The details of different techniques reported for yolk–shell microgels and their hybrids are described in Table 2.

5. Properties of yolk–shell microgels and hybrids

On the basis of structural constituents, the characteristics of yolk–shell microgels and their hybrids can be divided into two classes, *i.e.*, on the basis of a polymeric network, *i.e.*, the shell of the yolk–shell microgel system and on the basis of the yolk of the yolk–shell microgel system.

5.1 On the basis of the polymeric network

The polymeric network or shell of the yolk–shell microgels contain moieties that respond to the changes in the environmental stimuli. The details of the responsive behavior of yolk–shell microgels and their hybrids on the basis of polymeric network is given below. A brief summary of the properties of yolk–shell microgels on the basis of their polymeric network is described in Table 3.

5.1.1 Thermoresponsive yolk–shell microgels and their hybrids. The most widely reported thermoresponsive polymeric networks are made up of PNIPAM.[43,46,47,55,81] For PNIPAM microgels, there is a well-defined volume transition at a specific temperature of 32 °C in an aqueous medium called volume phase transition temperature (VPTT). This transition is reversible under cooling and heating cycles. A fractional change in the size of the microgel due to the absorption of water is called the swelling ratio $[(D_S/D_{DS})^3]$. The swelling ratio calculated from the data of dynamic light scattering (DLS) measurements proved the thermoresponsive behavior of PNIPAM microgels. When the temperature of the medium is increased, the hydrogen bond between the amide functionality of the PNIPAM microgels network and water is broken down, and the system changes

Table 2 Summary of various techniques employed for the characterization of yolk–shell microgels and their hybrids

Characterization technique	Applications	Composition of yolk–shell microgels and their hybrids	Ref.
Thermogravimetric analysis	The thermal stability of yolk–shell microgels was explored	P(MAA-*co*-EGDMA)@void@P(NIPAM-*co*-MAA)	48
		Fe_3O_4@void@PMAA	30
		Fe_3O_4@void@PMAA@void@PNIPAM	54
Energy dispersive X-ray (EDX) analysis	Mass content of metal in hybrid yolk–shell microgels was discovered	Ag@air@PMAA	75
X-ray photoelectron spectroscopy (XPS)	Concentration of metal in hybrid yolk–shell microgels was predicted	PS@void@PS-*co*-PMAA	77
		Fe_3O_4@void@PMAA@void@PNIPAM	54
Vibrating-sample magnetometry (VSM)	To determine the saturation magnetization of magnetic particles, present in yolk–shell microgels	Fe_3O_4@void@PMAA	78
		SiO_2–Fe_3O_4@void@P(BIS-*co*-MAA)	71
X-ray diffraction (XRD) spectroscopy	To determine the size of the nanostructure	Fe_3O_4@void@PMAA@void@PNIPAM	54
	To determine the crystal structure of nanoparticles of the yolk–shell hybrid. Microgels		
Dynamic light scattering (DLS)	To determine the D_h of yolk–shell microgels in swollen and de-swollen state	Au@void@PNIPAM	46
		PMAA@void@PNIPAM	50
		P(MAA-*co*-EDGMA)@void@PNIPAM	49
	To determine the size distribution of microgels	SiO_2–Fe_3O_4@void@P(BIS-*co*-MAA)	71
		Fe_3O_4@void@PMAA	79
Fourier transform infrared (FT-IR) spectroscopy	To determine the bonds present in the network of hybrid yolk–shell microgels	Ag@void@PMAA	75
		CPMAA@void@CPNIPAM	72
		Fe_3O_4@void@PMAA	78
		Fe_3O_4@void@PMAA@void@PNIPAM	54
		Au–Fe_3O_4@void@PNIPAM	80
		Fe_3O_4@void@PMAA	30
Scanning electron microscopy (SEM)	To determine the morphology of hybrid yolk–shell microgels	Fe_3O_4@void@PMAA	78
UV-visible spectroscopy	To determine the optical properties of hybrid yolk–shell microgels	CPMAA@void@CPNIPAM	72
	The dimensions of nanostructures were predicted		
Transmission electron microscopy (TEM)	The shape and size distribution of hybrid yolk–shell microgels was investigated	P(MAA-*co*-EGDMA)@void@P(NIPAM-*co*-MAA)	48
		PMAA@void@PNIPAM	50
		Au–Fe_3O_4@void@PNIPAM	80
		SiO_2–Fe_3O_4@void@P(BIS-*co*-MAA)	71

from hydrophilic to hydrophobic. This will result in a decrease in the hydrodynamic radius (R_h) of the polymeric network. Wu *et al.*[17] documented the fabrication of Au–PNIPAM yolk–shell hybrid microgels and studied their catalytic activity towards the reduction of 4-NP and nitrobenzene in response to changes in the temperature of the medium. The conversion of 4-nitrophenol (being hydrophilic in nature) is favored below VPTT because the Au–PNIPAM yolk–shell hybrid microgels system is

Table 3 Properties of yolk–shell microgels on the basis of their polymeric network and characterization

S. No.	System	Polymeric network	Property	Characterization	Ref.
1	Gold@void@poly(*N*-isopropylacrylamide) [Au@void@PNIPAM]	PNIPAM	Thermal response	DLS, UV-Vis, TEM	46
2	Poly(acrylic acid)@void@poly(2-hydroxyethylmethacrylate) [PAA@void@PHEMA]	PHEMA	Thermo-sensitivity	FT-IR, FE-SEM and TEM	53
3	Silica-magnetite@void@poly(*N*,*N*′-methylenebisacrylamide-*co*-methacrylic acid) [SiO_2–Fe_3O_4@void@P(BIS-*co*-MAA)]	MAA	pH sensitivity	TEM, FT-IR, DLS	71
4	Poly(ε-caprolactone)@void@poly(ε-caprolactone)/magnetite [PCL@void@PCL/Fe_3O_4]	PCL/Fe_3O_4	Magnetic	XRD, SEM, FT-IR	82
5	Poly(methacrylic acid-*co*-ethyleneglycol dimethacrylate)@void@poly(*N*-isopropylacrylamide) [P(MAA-*co*-EGDMA)@void@PNIPAM]	PNIPAM	Thermal response	DLS, TEM, FT-IR	49

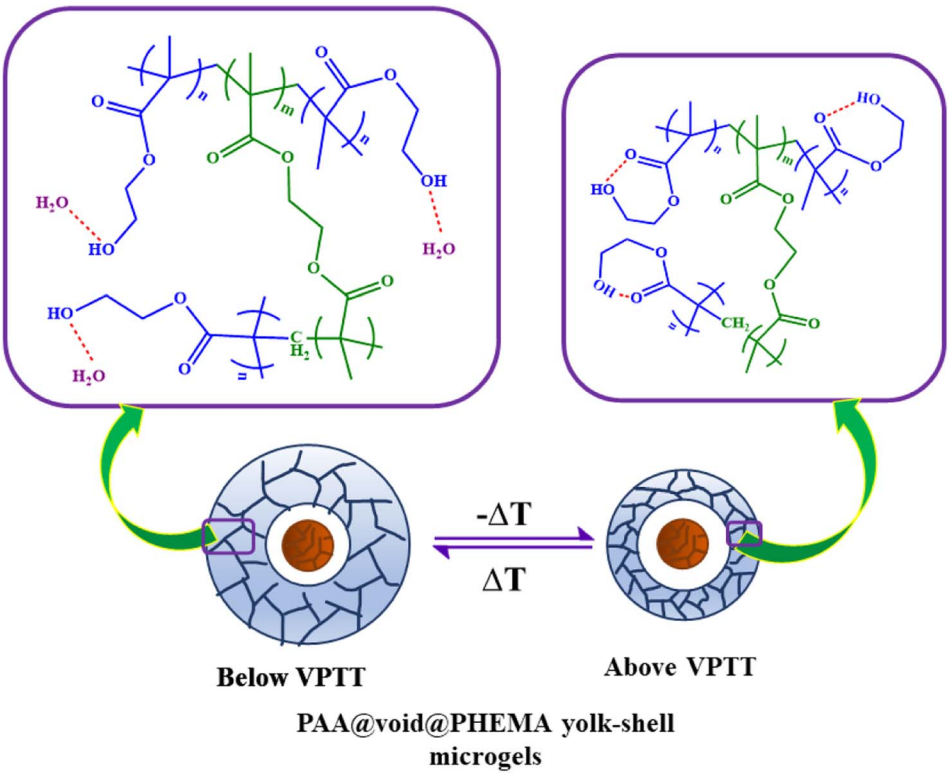

Fig. 12 Thermoresponsive behavior of PAA@void@PHEMA yolk–shell microgels; below VPTT, the outer shell is in a swollen state and intermolecular H-bonding dominates in PHEMA, while above VPTT, intramolecular H-bonding dominates and the polymeric system is in a deswollen state.

in the hydrophilic state. When the temperature is increased from the VPTT, Au–PNIPAM yolk–shell hybrid microgels system becomes hydrophobic with the loss of water and goes to a shrunken state, which favors the reduction of nitrobenzene (being hydrophobic in nature).

Nikravan *et al.*[65] have explored poly(acrylic acid)@void@poly(2-hydroxyethyl methacrylate) (PAA@void@PHEMA) yolk–shell polymeric system with the thermoresponsive PHEMA shell in terms of variation of absorbance with temperature. The thermosensitive behavior of PHEMA arises owing to competition between intermolecular and intramolecular hydrogen bonding at different temperatures. Below VPTT, there is an intermolecular hydrogen bonding between the carbonyl and hydroxyl groups of PHEMA with water (H_2O) and microgel is in the swollen state, *i.e.*, hydrophilic. When the temperature is increased above VPTT, intramolecular hydrogen bonding between the carbonyl functionalities and the hydroxyl group of PHEMA dominates. This results in the deswelling of the polymeric network and imparts hydrophobic properties to the microgel. The process is shown in Fig. 12. However, further investigation is still needed to prove the thermosensitive behavior of the PAA@void@PHEMA yolk–shell polymeric system in terms of the measurement of the change in the hydrodynamic diameter with temperature using DLS because PHEMA is generally supposed to be insensitive to temperature.

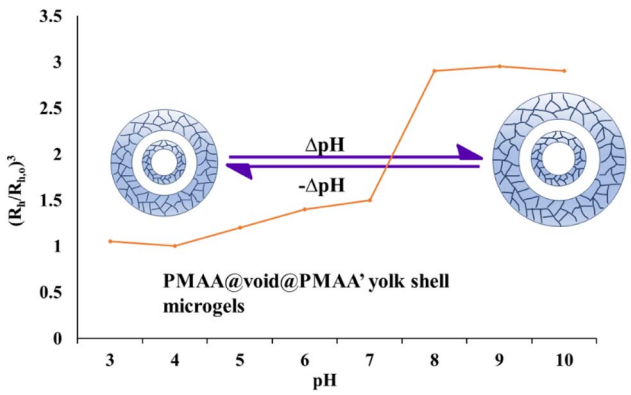

Fig. 13 The pH-responsive behavior of the PMAA@void@PMAA polymeric system; with an increase in the pH of the medium, the size of the polymeric system is also increased. The hydrodynamic volume also increases with an increase in the pH of the medium.

Wu *et al.*[22] documented the growth of Au yolk (15 nm, 67 nm, and 95 nm) in Au@PNIPAM yolk–shell microgels and studied the effect of temperature on the hydrodynamic diameter of these cross-linked yolk–shell polymeric systems. They noticed that there was a gradual decrease in the D_h values of all these yolk–shell microgels with the variation in the temperature of the medium.

5.1.2 pH-responsive yolk–shell microgels and their hybrids. The polymeric network, *i.e.*, the shell of the yolk–shell microgels may have some functionalities which can ionize, for example, the presence of some basic or acidic groups in them.

Owing to the presence of these functionalities, the yolk–shell microgels can respond to changes in the pH of the medium.[24] This property of yolk–shell microgels is called pH sensitivity.

Liu *et al.*[24] have reported the pH-sensitive poly(*N*,*N*′-methylenebisacrylamide-*co*-methacrylic acid) [P(BIS-*co*-MAA)] hollow polymeric microspheres with moveable magnetic/silica core and investigated their pH-sensitivity using DLS measurements. The hydrodynamic radius (R_h) of P(BIS-*co*-MAA) was 577 nm at pH = 3. With an increase in pH from 3 to 7, R_h increased to 640 nm. Further increase in the pH to 11 again increased the R_h to 742 nm. This increase in R_h was observed owing to the partial ionization of COOH functional groups of poly(methacrylic acid) [PMAA]. The repulsion in carboxylate (COO^-) ions and hydrophilic nature at higher pH values resulted in an increase in the R_h value.

Li *et al.*[44] investigated the pH sensitivity of multilayered hybrid yolk–shell polymeric system with different cross-linking density of PMAA. The hydrodynamic diameter (D_h) of PMAA@void@PMAA polymeric system was determined by DLS measurement and compared with single shell PMAA hollow microspheres. Both types of polymeric systems show a considerable increase in D_h with an increase in the pH of the medium. At higher pH, the COOH groups of PMAA are deprotonated and are in a swollen state. This size transition is reversible with variation in the pH of the medium. The PMAA shell with higher cross-linking density shows resistance to size variation. The swelling ratio ($(R_h/R_{h,4})^3$, $R_{h,4}$ = hydrodynamic radius at pH = 4) of PMAA (with lower cross-linking density) is increased by a factor of 3.9 when the pH is raised from 4 to 8, while PMAA (with higher cross-linking density) shows only an increase by 2.9 factor when the pH of the medium is raised from 4 to 8. The transition in the size of the prepared PMAA@void@PMAA polymeric system due to the variation in the pH of the medium is shown in Fig. 13.

5.1.3 Ionic strength responsive yolk–shell microgels and their hybrids. The polymeric shell of yolk–shell microgels may have ionizable functionalities. Such kind of yolk–shell microgels show size dependency on the ionic concentration in the medium. Li *et al.*[25] have reported silver@void@poly(methacrylic acid) [Ag@void@PMAA] hybrid nanorattles and investigated the effect of ionic strength on their size, as shown in Fig. 14. The outer shell of the prepared microgel is PMAA and it is pH sensitive. At a higher pH value, PMAA is completely ionized and exists in a swollen state. At this stage, it is highly sensitive to the ionic strength of the medium. There is a significant reduction in the size of the microgel when the concentration of sodium chloride (NaCl) in the medium is raised from 0.1 to 1.0 M. At a pH of 9.2, the COOH groups of PMAA are completely ionized. There is an electrostatic force of repulsion between the COO^- groups, which allows the shell to adopt a swollen state. When the concentration of salt (NaCl) is increased from 0.1 to 1.0 M,

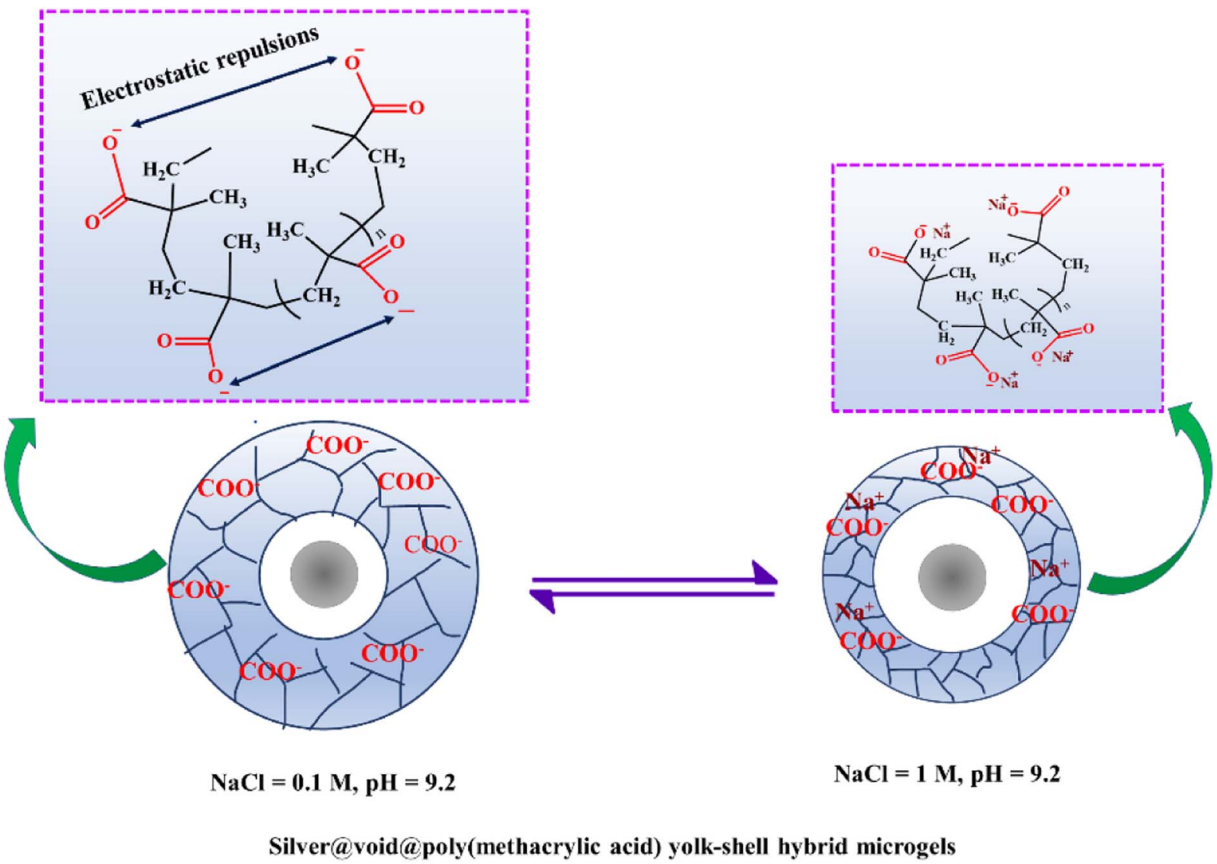

Fig. 14 Effect of increasing salt concentration on the size of the polymeric network. With an increase in the salt concentration, the size decreases due to the presence of oppositely charged ions to counter the repulsive effect.

Table 4 Characteristics of yolk–shell microgels on the basis of the nature of the yolk and their characterization

S. No.	System	Yolk	Property	Characterization	Ref.
1	Poly(methacrylic acid-*co*-ethyleneglycol dimethacrylate)@void@poly(*N*-isopropylacrylamide-*co*-methacrylic acid) [P(MAA-*co*-EDGMA)@void@P(NIPAM-*co*-MAA)]	P(MAA-*co*-EDGMA)	pH sensitivity	TGA, TEM FT-IR	48
2	Polymethacrylic acid@void@poly(*N*-isopropylacrylamide) [PMAA@void@PNIPAM]	PMAA	pH sensitivity	FT-IR, TEM FE-SEM	55
3	Polyacrylic acid@void@poly(2-hydroxyethyl methacrylate) [PAA@void@PHEMA]	PAA	pH sensitivity	FT-IR, FE-SEM TEM	65
4	Silver@void@microporous polymer nanoparticles [Ag@void@MPNPs]	Ag	Antibacterial activity	XRD, UV-Vis, DLS	83
5	Magnetite@void@polymethyl methacrylate [Fe_3O_4@void@PMMA]	Fe_3O_4	Magnetic behavior	VSM, SEM, TEM, XRD, TGA	78
6	Magnetite/silica@void@poly(*N*,*N*′-methylenebisacrylamide-*co*-methacrylic acid) [Fe_3O_4/SiO_2@void@P(BIS-*co*-MAA)]	Fe_3O_4/SiO_2	Magnetic behavior	TEM, FT-IR, VSM, DLS	71
7	Magnetite@void@poly(acrylic acid-*co*-ethylene glycol dimethacrylate) [Fe_3O_4@air@P(AA-EGDMA)]	Fe_3O_4	Magnetic behavior	TEM, TGA, FT-IR, XRD	84
8	Magnetite@void@poly[(ethyleneglycol dimethacrylate)-*co*-(*N*-vinylcarbazole)] [Fe_3O_4@void@P(EGDMA-*co*-NVCz)] microspheres	Fe_3O_4	Magnetic behavior	FT-IR, TEM, VSM, UV-Vis, florescence spectroscopy	85

more sodium ions (Na^+) are available to counter the charge on carboxylate ions. This shielding of charge reduces the osmotic pressure and internal repulsion in the shell, leading the PMAA shell to a de-swollen state.

5.2 On the basis of yolk

Various properties of yolk–shell microgels and their hybrids depend upon the type of the yolk present in yolk–shell polymeric system, such as pH sensitivity, antibacterial, magnetic and optical properties. The yolk[55] of the yolk–shell microgels may have few ionizable moieties like carboxyl (COOH) groups and amine functionalities, which get protonated or deprotonated by a variation in the pH of medium, gives pH sensitivity to yolk–shell microgels. Du *et al.*[49] have documented poly(methacrylic acid-*co*-ethyleneglycol dimethacrylate)@void@poly(*N*-isopropylacrylamide) [P(MAA-*co*-EDGMA)@void@PNIPAM] yolk–shell microspheres and discussed their pH-sensitive behavior. DLS was employed to determine the effect of media pH on the D_h value of P(MAA-*co*-EDGMA) the yolk of yolk–shell microgels. They observed that at 25 °C, when the pH of medium was varied from pH = 3 to pH = 11, D_h increased gradually from 150 nm to 224 nm. This increase in hydrodynamic diameter results owing to electrostatic repulsion present between the carboxyl anions of poly(methacrylic acid) [PMAA] component of the P(MAA-*co*-EDGMA) yolk of yolk–shell microgels. As the pH or alkalinity of the solution increases, carboxyl functionalities ionize into carboxyl anions, resulting in more hydrophilic and extended chains of PMAA.

Wu *et al.*[47] have elaborated gold-poly(*N*-isopropylacrylamide) [(Au–PNIPAM)] yolk–shell microgel particles and discussed the optical properties of the yolk–shell microgel system that arises due to the presence of the Au yolk. One of the most captivating features of Au–PNIPAM yolk–shell composites is surface plasmon resonance wavelength (λ_{SPR}) that can be tuned by varying the temperature of the medium. For Au–PNIPAM yolk–shell composites, the value of λ_{SPR} was found to be 547 nm at 15 °C in aqueous medium and is shifted to increased wavelength (λ_{SPR} = 557 nm) when the temperature is increased up to 50 °C. This increment in value of λ_{SPR} with an increase in the temperature of the medium is caused by an increase in the local refractive index around the Au yolk nanoparticles as a result of volume phase transition (VPT) of Au–PNIPAM yolk–shell composite system. On account of this variation in λ_{SPR} with a variation in temperature, optical temperature sensors can be developed. Table 4 shows the properties of yolk–shell microgels on the basis of the nature of the yolk and their characterization.

6. Applications

6.1 Catalytic applications

Catalysts provide an accelerated path toward the desired product with lower activation energy. The most widely used catalysts are MNPs with higher surface area and recyclability.[86–88] One of the major challenges linked with the utilization of bare metal nanoparticles as catalysts is their aggregation owing to the high surface energy they possess. This reduces the surface area for catalysis and hence the productivity. To avoid this problem, yolk–shell nanostructures have been reported as stable and effective catalysts because of their structure-based novel properties.[88,89] Although the introduction of a shell prevents aggregation and provides stability to the

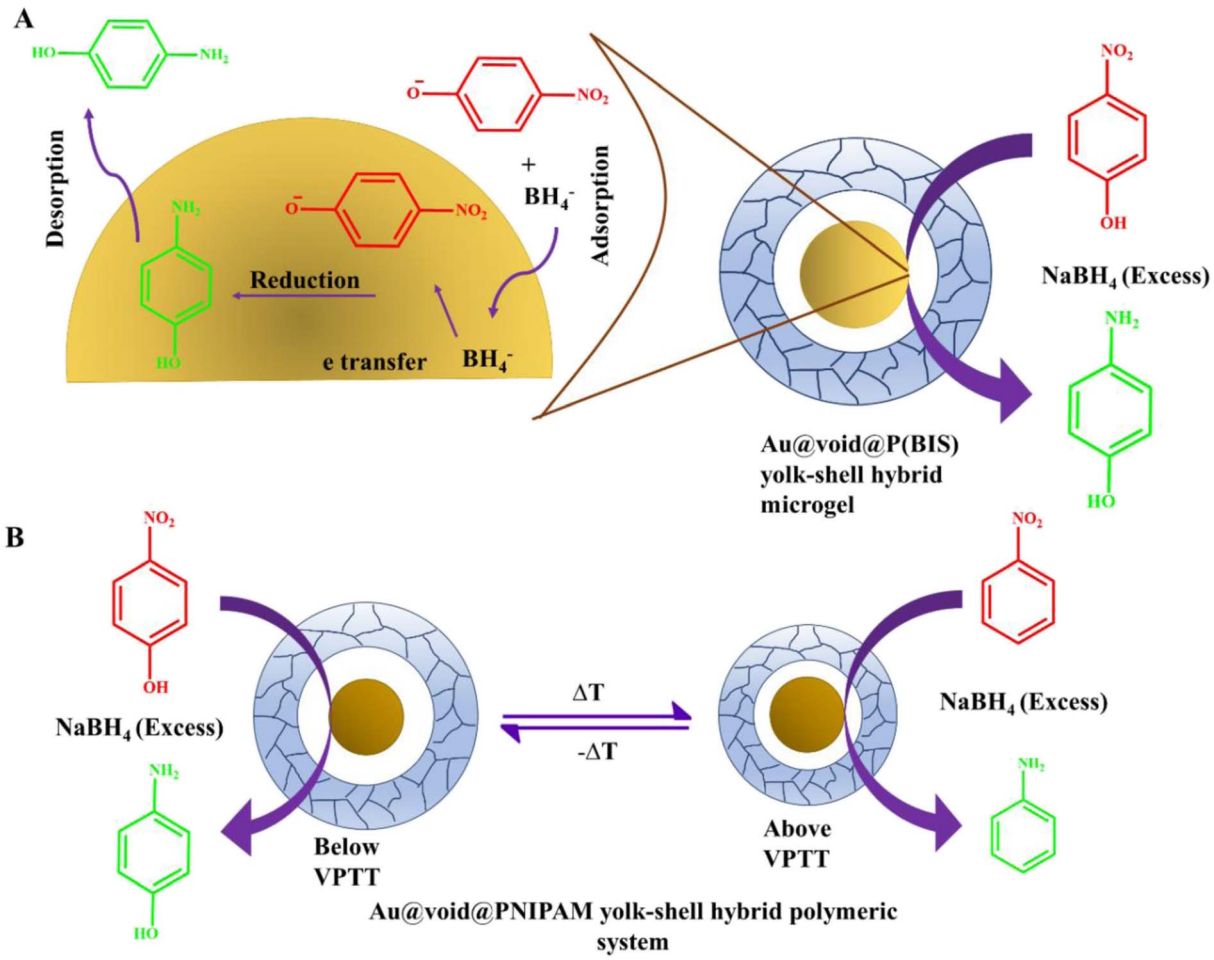

Fig. 15 (A) The mechanism of reduction of 4-NP to 4-AP using the Au@void@P(BIS) hybrid polymeric system. The reduction of 4-NP follows the Langmuir–Hinshelwood mechanism. (B) The thermo-responsive selectivity of Au@void@PNIPAM yolk–shell hybrid microgels. Below VPTT, the reduction of 4-NP is favorable due to the hydrophilic nature of the polymeric network and above VPTT, the reduction of NB is favorable because of the hydrophobic nature of the polymeric network.

nanoparticles (NPs), it delays the encounter of the reactant molecules with the NPs because of the thick shell and reduces the catalytic activity.

Thus, to address the previously mentioned issues and enhance both stability and efficiency of NPs-based catalysts, the outer shell around catalytically active metallic core should be porous, and there should be free space like the yolk system of an egg between the metallic core and the outer porous shell that will provide room to reactants for reaction. If the outer shell is a cross-linked polymeric network, then the system is called a yolk–shell hybrid microgel. Yolk–shell hybrid microgels with efficient and stable catalytic activities are widely reported in the literature.[25,28,31,32,62] Liu *et al.*[28] have explored the fabrication of Au–poly(*N*,*N*′-methylenebisacrylamide) [Au–P(BIS)] yolk–shell system with movable Au yolk and investigated its catalytic activity using a model reaction of transformation of 4-nitrophenol (4-NP) to 4-aminophenol (4-AP) in the presence of an excess of sodium borohydride ($NaBH_4$). To investigate the catalytic applications, a yellow-colored solution of 4-NP and $NaBH_4$ having UV-Vis absorption at 400 nm (λ_{max} associated with 4-nitrophenolate ions) was taken in a cuvette to monitor the variation in the absorbance value at 400 nm. No significant shift in the value of absorbance at 400 nm was noticed. Then, the Au@void@P(BIS) yolk–shell microgel was added to the solution, the yellow color of the solution started to disappear and a new peak at 300 nm (λ_{max} linked with 4-AP) in UV-Vis spectra appeared, confirming the conversion of 4-NP to 4-AP. In the absence of Au@void@P(BIS), BH_4^- does not possess enough energy to reduce 4-NP. When Au@void@P(BIS) is added to the solution, BH_4^- and 4-nitrophenolate ions diffuse into the polymeric system, and a reaction is initiated by the shifting of the electron from BH_4^- to 4-nitrophenolate ion on the surface of the Au core. The product 4-AP then desorbs from the surface of Au and diffuses out of the P(BIS) shell, as shown in Fig. 15(A). The value of the apparent rate constant (k_{app}) was predicted by applying pseudo first order kinetic model as given in the equation below.

$$-\frac{dC_t}{dt} = k_{app}C_t \quad (1)$$

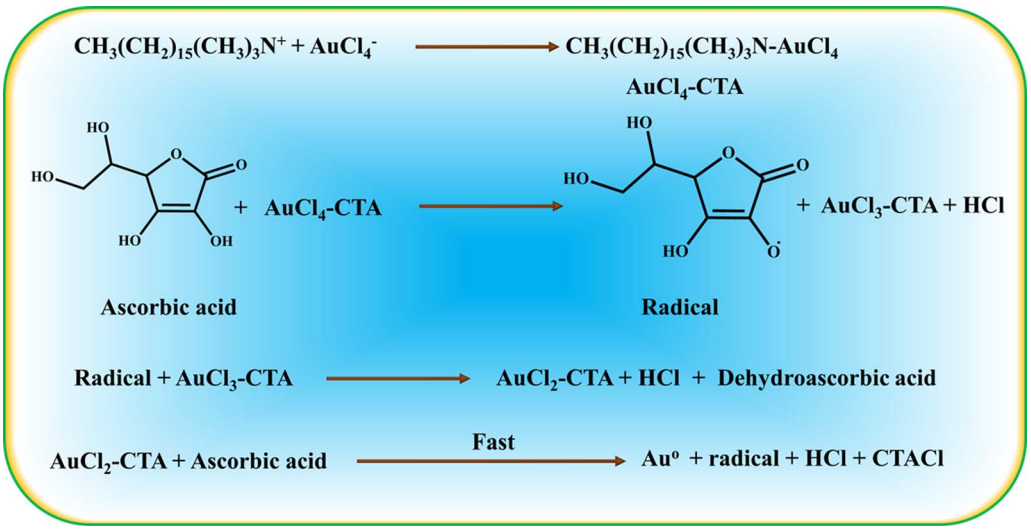

Scheme 1 The mechanism of reduction of Au(III) with ascorbic acid for the growth of Au yolk of Au@void@PNIPAM in the presence of CTAB.

Here, C_t is the concentration of 4-NP at any time t, and k_{app} is the apparent rate constant that can be determined from the slope of $\ln\frac{C_t}{C_0}$ *versus* time plot.

The yolk–shell hybrid polymeric system with stimuli tunable selectivity of catalytic activity has also been reported in the literature.[17,56] Wu *et al.*[17] have explained Au@void@PNIPAM yolk–shell microgels with temperature-dependent tunable selectivity for catalysis. PNIPAM has a VPT temperature of 32 °C in aqueous medium. Below this value of temperature, PNIPAM has a hydrophilic nature and exists in a swollen state. Hence, below VPTT, 4-NP molecules, being hydrophilic in nature, can diffuse into the shell and get reduced to 4-AP in the presence of an excess of $NaBH_4$. When the temperature is increased from VPTT, the polymeric shell obtains a hydrophobic nature and acquires a de-swollen state. Under these conditions, 4-NP cannot penetrate into the polymeric system, but the reduction of hydrophobic nitrobenzene (NB) to aminobenzene (AB) is favored. Thus, at a temperature lower than VPTT, 4-NP is reduced faster, and at a temperature higher than VPTT, NB is reduced faster in aqueous medium. The reduction of 4-NP and NB at different temperatures is shown in Fig. 15(B).

Jia *et al.*[90] have reported Au@void@PS and Pt@void@PS nanocapsules and studied their catalytic activity for multiple reactions. Au@void@PS nannocapsules were used for the oxidation of benzaldehyde and benzyl alcohol while the Pt@void@PS nanocapsules were employed for the hydrogenation of cyclohexene. The catalytic activity of Au@void@PS and Pt@void@PS nanocapsules was compared with bare Au NPs and Pt NPs. The yolk–shell structured nanocapsules showed efficient catalytic activity.

6.2 Nanoreactors

Yolk–shell microgels and their hybrids can be employed as nanoreactors for the preparation and stabilization of

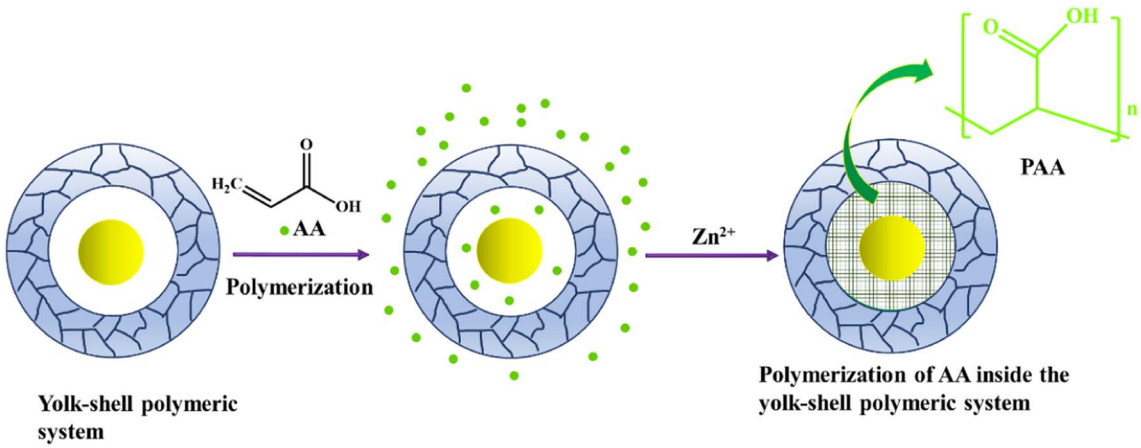

Fig. 16 The fabrication of acrylic acid inside the polymeric yolk–shell microgels by thermal polymerization in the presence of Zn^{2+} as a physical cross-linker.

nanoparticles. Wu *et al.*[22] have discussed the fabrication of Au@void@PNIPAM yolk–shell microgels having movable yolk and used this system as a nanoreactor for the further growth of Au nano yolk. The movable yolk of the prepared polymeric system is used as a seed for the further growth of Au NPs by the reduction of tetrachloroauric acid ($HAuCl_4$) using ascorbic acid (AA) as a reductant in the presence of cetyltrimethyl ammonium bromide (CTAB). CTAB provides stability and prevents secondary nucleation in the solution. AA, being a mild reductant, reduces Au(III) to Au(I) oxidation state in the presence of CTAB. The use of already prepared Au yolk as the seed favors the catalytic reduction of Au(I) particles to Au^0 NPs on the surface of the yolk, as shown in Scheme 1. The increase in the size of Au yolk was proved by TEM investigation of the hybrid system.

Guo *et al.*[69] have discussed the fabrication of poly(acrylic Acid) (PAA) gels in aqueous void space between the yolk and polymeric shell of the yolk–shell polymeric system. The water-soluble monomer acrylic acid (AA) units have a small size and can easily diffuse into the polymeric shell. The thermal polymerization of AA produces anionic polyelectrolyte (PAA), which cannot diffuse out of the polymeric shell. PAA polymerizes inside and outside of the polymeric network producing a hard-boiled yolk–shell morphology when the buffer containing divalent zinc ions is added, which acts as a physical cross-linker to form PAA hydrogel in the void of the yolk–shell system, as shown in Fig. 16. These results confirmed the ability of the yolk–shell polymeric systems to carry out chemical reactions within the yolk–shell microgel system to produce a new useful polymeric system.

6.3 Antibacterial activity

Du *et al.*[32] have reported a yolk–shell polymeric network with silver (Ag) yolk and studied their antibacterial activity against *Escherichia coli* (*E. coli*) and *Staphylococcus aureus* (*S. aureus*) using bacterial inhibition ring test. Antibacterial tests were conducted over 10 to 60 hours of bacterial culturing. Two samples were tested for antibacterial activity, one was blank and the other with the yolk–shell polymeric network. Bacteria continuously grew around blank sample, but no growth around the Ag-yolk based polymeric network was observed over 60 hours of time. Most of the antibacterial agents possessed antibacterial activity for 24 hours. But this system sustained activity for 60 hours with good efficiency.

The mechanism of antibacterial activity of Ag NPs is built on the release of Ag^+ ions by the oxidation of Ag^0 in acidic medium. The yolk–shell polymeric system sustains the release of Ag^+. As the bacterial membrane is acidic in nature and possesses an oxidizing environment, thus, this accelerates the conversion of Ag NPs to Ag^+ (Fig. 17). A higher concentration of Ag^+ disrupts the outer membrane of the bacteria and leads to a reduction in the cell viability, ultimately killing the bacteria. The driving force behind the penetration of Ag^+ ions into the cell wall is a strong interaction between Ag^+ ions and thiol groups of cysteine proteins in the cell wall of the bacteria. The collection of Ag^+ ions in the cell wall causes the formation of pits in the cell wall and ultimately destroys the bacterial cell wall. The rate of bacterial killing is linked to the rate of change of mass of Ag yolk, which ultimately depends upon the concentration of oxygen, hydrogen ions, Ag content and temperature of medium, as shown in Fig. 17.

6.4 Drug delivery

Microgels possess three-dimensional cross-linked polymeric network and have the ability to hold a large amount of solvent, mostly water. This property of the microgels makes them biocompatible and a potential member for drug delivery systems (DDS). One of the main issues associated with these systems and other conventional systems is that they cannot distinguish between affected and unaffected cells and have detrimental effects. For example, most of the cancerous cells have pH value in the range of 6.0 to 7.0, while blood and normal tissues have a pH of 7.4.[91] Owing to this pH change, smart polymeric networks have gained wide attention in stimulus-responsive tunable controlled drug delivery.[92,93] Recently, the yolk–shell polymeric networks attracted the attention devising modern DDS with more control over drug uptake and release and higher efficiency.[30,42,51,59,63,65,94] Du *et al.*[23] have discussed the fabrication of multi-responsive yolk–shell polymeric DDS. The

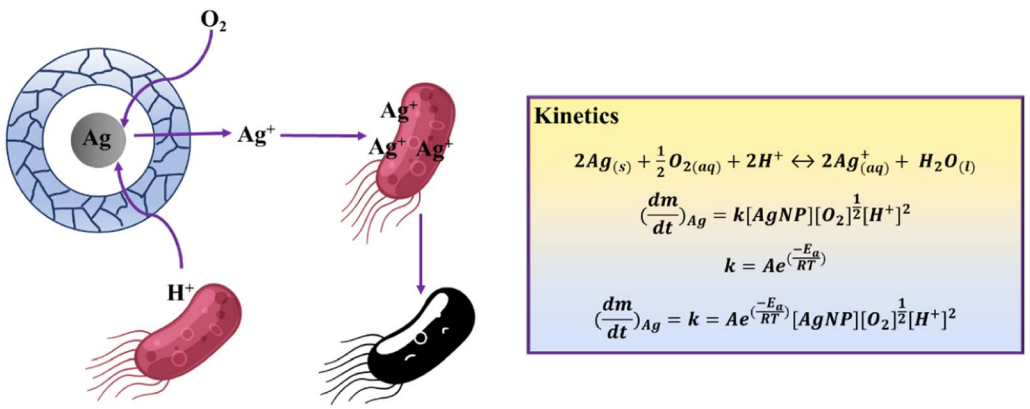

Fig. 17 Pictorial view of the antibacterial activity of Ag-based yolk–shell polymeric systems and the kinetics of oxidation of Ag NPs to Ag^+ ions, the actual warriors.

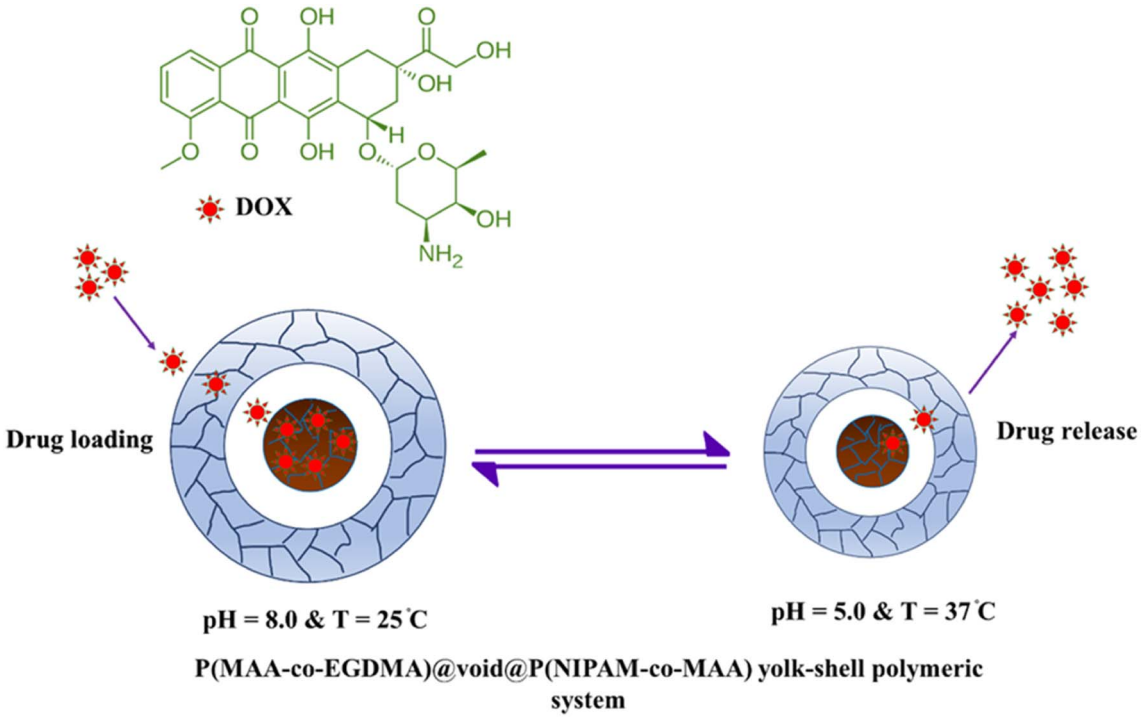

Fig. 18 The drug loading and drug releasing of the yolk–shell polymeric network P(MAA-*co*-EGDMA)@void@P(NIPAM-*co*-MAA) at different pH values and temperatures.

prepared yolk–shell polymeric network [P(MAA-*co*-EGDMA)@void@P(NIPAM-*co*-MAA)] was tested for drug delivery applications using 4-substituted-2,5-dimethoxyamphetamines (DOX) (an anticancer drug) as a model drug to be delivered. The yolk of this polymeric system is pH-responsive; with an increase in the pH of the medium, the drug uptake capacity also increases. When the pH increases from 5.0 to 10.0, the drug loading capacity (DLC) (calculated using eqn (2)) is increased from 2.91 wt% to 27.03 wt%. The drug loading capacity reaches its peak value at pH = 8.0, while decreasing the pH value to 5.0 lowered the drug loading capacity because of the unavailable electrostatic interaction between the carboxyl functionalities of the polymeric yolk and positively-charged DOX. The effect of electrostatic interactions is negligible; in fact, DOX loading is a physical process and follows the adsorption mechanism. At high pH, the yolk is in a swollen state and has large meshes; thus, DOX can easily penetrate into it. The release phenomenon is inverse to this: with a decrease in pH, the polymeric yolk deswells and the drug is forced to move out. At 37 °C, with a decrease in pH from 7.4 to 5.0, the percentage increase in drug release from 27.1% to 67% is observed in 47.5 hours. The presence of an outer polymeric shell hinders the drug release. But in the current scenario, the outer polymeric shell is P(NIPAM-*co*-MAA), which is temperature-responsive and has a VPPT of 32 °C, which is lower than the body temperature, *i.e.*, 37 °C. At this temperature, the outer polymeric shell also shrinks and helps to increase the drug release efficiency. Moreover, by increasing the cross-linking density of the polymeric yolk, the drug release capacity also increases. The drug loading and releasing of the yolk–shell polymeric system is shown in Fig. 18.

$$\text{DLC} = \frac{\text{weight of drug loaded in yolk (mg)}}{\text{total weight of yolk (mg)}} \times 100 \quad (2)$$

6.5 Lithium–sulfur batteries

Rechargeable batteries have gained the attention of modern-day studies because of their wide usage from daily life to industries. Different types of rechargeable batteries have been reported.

Table 5 The adsorption of metal ions at different pH values

Amount of metal ions adsorbed [q_e (mmol g^{-1})] for different metals	pH of the medium					
	2	3	4	5	6	7
Cu^{2+}	0.74	1.0	2.38	3.72	3.3	2.11
Pb^{2+}	0.40	0.7	1.21	2.35	2.48	1.82
Cr^{3+}	0.37	0.61	1.17	1.61	2.41	1.78
Cd^{2+}	0.28	0.43	0.76	0.81	1.2	0.74

Among these, lithium–sulfur (Li–S) batteries are considered as a suitable candidate to hold the position of modern-day energy storage systems owing to their large theoretical energy density of 2600 W h kg^{-1} (ref. 95) and environment-friendly nature, abundance and cost-effectiveness of sulfur.[96] The yolk–shell structures have been reported in the literature for energy storage applications.[97] The protection of the yolk of the yolk–shell structures by the shell and the empty space between the shell and yolk make them suitable for energy storage applications. However, the main problem with sulfur-based storage batteries is the low loading of sulfur on the yolk–shell system. To counter this problem, Zhang *et al.*[33] have reported sulfur@void@polypyrrole [S@void@PPy] hydrogels and used them as storage material for Li–S batteries. A coil cell system was used to measure the electrochemical performance of the prepared yolk–shell composites. A mixture of the yolk–shell composite, polyvinylidene fluoride (adhesive) and carbon black was formed. Then, *N*-methyl-2-pyrrolidone (NMP) was mixed to this mixture and agitated. A slurry was formed and transferred on Al foil and heated in a vacuum at 60 °C for 12 hours. A glove box filled with pure argon was used to assemble the cells. The counter electrode and separator were made of Li foil and polyethylene film, respectively. The electrolyte [$LiN(CF_3SO_2)_2$(LiTFSI) in a mixture of 1,3-dioxolane and 1,2-dimethoxyethane] was added to the cells. Electrochemical studies proved the good reproducibility and efficient stability of the yolk–shell composites. The cyclic charging and discharging performance were measured and compared with other systems (S@PPy composites). S@void@PPy showed better cyclic performance because of the void between sulfur and the PPy shell. The details of charging and discharging phenomenon and interpretation of the electrochemical parameters of the Li–S batteries are beyond the scope of this review.

These novel S@void@PPy hydrogels served as the best candidate for Li–S batteries because of the following reasons.

(i) They contained sulfur as the core with a high percentage about 98.4%.

(ii) The volume-change of sulfur during the cycling process is facilitated by the voids between the yolk and shell of the composite.

(iii) The shuttle effect is minimized as polysulfides were absorbed by PPy.

6.6 Adsorption of metal ions

The concentration of heavy metal ions in the environment is increasing day-by-day. These metal ions are indestructible and get accumulated in living organisms, causing serious health issues. Researchers apply various methods like ultra-filtration,[98] ion-exchange,[99] phyto-extraction,[100] reverse osmosis,[101] electrodialysis[101] and precipitation[102] for the elimination of metal ions from aqueous medium. Yolk–shell microgel systems can also be used for the extraction of heavy metal ions from aqueous medium. For example, Zhao *et al.*[26] reported a pH-responsive yolk–shell Fe_3O_4@void@PMAA hybrid polymeric system for the adsorption of metal ions. Because PMAA has a large amount of COOH groups, the hydrophilic permeable shell, void space in yolk–shell system and cost effectiveness make Fe_3O_4@void@PMAA hybrid polymeric system a suitable candidate for the adsorption of metal ions. The adsorption of copper(II) ions (Cu^{2+}), lead(II) ions (Pb^{2+}), chromium(III) ions (Cr^{3+}), and cadmium(II) ions (Cd^{2+}) on Fe_3O_4@void@PMAA hybrid polymeric system were studied at various pH values of the medium, as shown in Table 5. When the pH is increased from 2 to 5, there is an increase in the adsorption concentration, but when the pH reached 7, the adsorption decreases. The optimum pH for adsorption was between 5.0 and 6.0. When the pH was lower than 3.0, the PMAA shell is in protonated form and hinders the adsorption of metal ions on the polymeric network. With an increase in pH to 5.0, PMAA molecules were deprotonated with a swollen network and there was an electrostatic force of attraction between metal ions and COO^- groups; hence, adsorption was optimum. A further increase in the pH reduces the adsorption of metal ions because of the formation of metal hydroxide. This adsorbent system was compared with other microgel systems used for the adsorption of metal ions and was proved to be the best one among them.

The amount of metal ions adsorbed on the yolk shell hybrid system was calculated by the following equation.

$$q_e = \frac{(C_0 - C_e) \times V}{W \times A} \quad (3)$$

where C_0 and C_e are the initial and equilibrium amounts of metal ions (mg L^{-1}), respectively, V corresponds to the volume of metal ion solution (L), A denotes relative atomic weight of metal ions (mg $mmol^{-1}$) and W stands for the weight of the adsorbent (g).

7. Conclusion and future directions

Yolk–shell microgels have hollow solvent layer between the core and shell materials due to which the interference of the core and shell material in volume transitions can be avoided efficiently; this is why the yolk–shell microgels show independent multi-responsive property. During drug loading, the presence of a hollow layer between the core and shell materials in yolk–shell microgels allows ample room for the expansion of core materials. Thus, the yolk–shell microgels are best known for high drug loading capacity. Moreover, yolk–shell microgels and their hybrids are being used in the field of catalysis, lithium-ion batteries, anti-bacterial activity, for the adsorption of heavy metal ions and many more. This review briefly describes the synthesis of yolk–shell microgels and their hybrids, their peculiar properties, reactivity to diverse environmental stimuli and their utilization across multiple domains. For the synthesis of yolk–shell microgels, a readily detachable middle layer is required that can be etched employing the reagent known as the etching agent under optimized conditions. New researchers who are working in the area of cross-linked polymeric systems may find this article helpful as it gives a review of research advancement in the area of yolk–shell microgels. New techniques for the synthesis of yolk–shell microgels with desirable characteristics could be expanded upon in subsequent studies. A lot of literature on thermo-responsive yolk–shell microgels

deals with NIPAM. Future studies may involve the utilization of the monomer apart from NIPAM for the synthesis of thermosensitive yolk–shell microgel systems. Very few reports are discussed on the synthesis of Ag[25] and Pd[56] nanoparticles as the yolk of yolk–shell microgels. The fabrication of nanoparticles of other noble metals like Rh and Ni to be used as the yolk of yolk–shell microgels may be executed subsequently. The catalytic efficiency of Ni and Rh nanoparticles-based the yolk of the yolk–shell microgels may be investigated. Different organic conversions may occur in the availability of Ni and Rh nanoparticles-based yolk of yolk–shell microgels to get fine chemicals. Bimetallic nanoparticles may also be used as the yolk of yolk–shell microgels in the future. The polymeric network of yolk–shell microgels causes hindrance in the inward and outward movement of reactant for catalytic activity; thus, a probable solution for this problem can also be addressed in the future. A detailed investigation of the optical characteristics of plasmonic nanoparticles as the yolk of yolk–shell microgels may spark interest in forthcoming studies.

Abbreviations and symbols

AA	Ascorbic acid
AB	Aminobenzene
AIBN	2,2′-Azobisisobutyronitrile
Ag	Silver
AN	Acetonitrile
APM	3-Aminopropyl trimethosysilane
APTES	3-Aminopropyl triethylsilane
APS	Ammonium persulfate
Au	Gold
BIS	*N*,*N*′-Methylenebisacrylamide
CLSM	Confocal laser scanning microscopy
CMAA	Cross-linked poly(methacrylic acid)
COO^-	Carboxylate ion
COOH	Carboxylic acid
CPNIPAM	Cross-linked poly(*N*-isopropylacrylamide)
CTAB	Cetyltrimethyl ammonium bromide
Cd^{2+}	Cadmium(II) ion
Cr^{3+}	Chromium(III) ion
Cu^{2+}	Copper(II) ion
DDS	Drug delivery systems
DEG	Diethylene glycol
DLC	Drug loading capacity
DLS	Dynamic light scattering
DOX	4-Substituted-2,5-dimethoxyamphetamines
DVB	Divinyl benzene
d-PMAA	Disulfide cross-linked poly(methacrylic acid)
EDGMA	Ethylene glycol dimethacrylate
EDS	Energy dispersive spectrometer
EDX	Energy dispersive X-ray
EG	Ethylene glycol
EtOH	Ethanol
E. coli	*Escherichia coli*
$FeCl_3 \cdot 6H_2O$	Iron(III) chloride hexahydrate
Fe_3O_4	Magnetite
FESEM	Field emission scanning electron microscopy
FT-IR	Fourier transform infrared spectroscopy
$HAuCl_4$	Tetrachloroauric acid
HD	Hexadecane
HEMA	2-Hydroxyethyl methacrylate
HF	Hydrofluoric acid
H_2O	Water
ICP	Inductively coupled plasma
KPS	Potassium persulfate
LIBs	Lithium-ion batteries
MAA	Methacrylic acid
MNPs	Metal nanoparticles
MPNPs	Microporous polymers nanoparticles
MPS	3-(Methacryloxy)propyl trimethoxysilane
$NaBH_4$	Sodium borohydride
NaCl	Sodium chloride
NaOH	Sodium hydroxide
NB	Nitrobenzene
NIPAM	*N*-Isopropylacrylamide
NPs	Nanoparticles
NH_3	Ammonia
NH_4OAc	Ammonium acetate
Na^+	Sodium ion
O/W	Oil-in-water
PAA	Poly(acrylic acid)
PBzMA	Poly(benzyl methacrylate)
PCL	Poly(ε-caprolactone)
Pd	Palladium
PGA	Poly(γ-glutamic acid)
PISR	Polymerization-induced self-assembly and reorganization
PMAA	Poly(methacrylic acid)
PNIPAM	Poly(*N*-isopropylacrylamide)
PPy	Polypyrrole
PVDMA	Poly(2-vinyl-4,4-dimethyl azlactone)
PVP	Poly(vinylpyrrolidone)
P(BIS)	Poly(*N*,*N*′-methylenebisacrylamide)
P(CMSt)	Poly(4-vinylbenzylchloride)
P(DVB)	Poly(divinylbenzene)
P4VP-TC	*S*-1-dodecyl-*S*-(α,α′-dimethyl-α″-acetic acid)-trithiocarbonate-terminated poly(4-vinylpyridine)
Pb^{2+}	Lead(II) ion
RAFT	Reversible addition–fragmentation chain transfer
R_h	Hydrodynamic radius
RS-CPMAA	Raspberry-shaped cross-linked poly(methacrylic acid)
SDS	Sodium dodecyl sulfate
SEM	Scanning electron microscope
SiO_2	Silica
SS	Sodium silicate
St	Styrene
S. aureus	*Staphylococcus aureus*
TEM	Transmission electron microscopy
TEOS	Tetraethyl orthosilicate
TGA	Thermogravimetric analysis
UV-Vis	Ultraviolet-visible
u-PMAA	Uncross-linked poly(methacrylic acid)
VPT	Volume phase transition
VPTT	Volume phase transition temperature
VSM	Vibrating sample magnetometer

XPS	X-ray photoelectron spectroscopy
XRD	X-ray diffraction
YSMs	Yolk–shell microspheres
Zn^{2+}	Zinc(II) ion
4-AP	4-Aminophenol
4-NP	4-Nitrophenol

Conflicts of interest

Authors declare no conflict of interest.

Acknowledgements

The authors thankfully acknowledge the financial support from the Royal Society of Chemistry (RSC), UK under RSC Research Fund (R22-6381055435) for the year 2022–2023 to carry out the research activities at University of the Punjab, New Campus, Lahore 54590, Pakistan. S. Zhou is thankful to the NIDDK-NIH for funding (Award Number: 1R15DK127360-01A1). A. Irfan extends his appreciation to the Deanship of Scientific Research at King Khalid University for support through the small research groups program (R.G.P1/38/44). A. R. Chaudhry is grateful to the Deanship of Graduate Studies and Scientific Research at the University of Bisha for supporting this work through the Fast-Track Research Support Program.

References

1 J. Liu, S. Z. Qiao, J. S. Chen, X. W. D. Lou, X. Xing and G. Q. M. Lu, *Chem. Commun.*, 2011, **47**, 12578–12591.
2 S. Xing, L. H. Tan, T. Chen, Y. Yang and H. Chen, *Chem. Commun.*, 2009, **13**, 1653–1654.
3 J. Liu, J. Cheng, R. Che, J. Xu, M. Liu and Z. Liu, *ACS Appl. Mater. Interfaces*, 2013, **5**, 2503–2509.
4 S. Wang, M. Zhang and W. Zhang, *ACS Catal.*, 2011, **1**, 207–211.
5 X. Chen, L. Song, X. Li, L. Zhang, L. Li, X. Zhang and C. Wang, *Chem. Eng. J.*, 2020, **389**, 124416.
6 L. Gao, J. Fei, J. Zhao, W. Cui, Y. Cui and J. Li, *Chem.–Eur. J.*, 2012, **18**, 3185–3192.
7 J. Liu, Y. Zhou, J. Wang, Y. Pan and D. Xue, *Chem. Commun.*, 2011, **47**, 10380–10382.
8 G. Li, Y. Chen, L. Zhang, M. Zhang, S. Li, L. Li, T. Wang and C. Wang, *Nano-Micro Lett.*, 2018, **10**, 1–11.
9 J. Liang, F. Teng, T. M. Chou and M. Libera, *Polymer*, 2017, **116**, 1–4.
10 A. Fernández-Barbero, I. J. Suárez, B. Sierra-Martín, A. Fernández-Nieves, F. J. de Las Nieves, M. Marquez, J. Rubio-Retama and E. López-Cabarcos, *Adv. Colloid Interface Sci.*, 2009, **147**, 88–108.
11 S. V. Vinogradov, *Curr. Pharm. Des.*, 2006, **12**, 4703–4712.
12 N. Welsch, M. Ballauff and Y. Lu, *Chemical Design of Responsive Microgels*, 2010, 129–163.
13 T. Hellweg, *J. Polym. Sci., Part B: Polym. Phys.*, 2013, **51**, 1073–1083.
14 I. Berndt, J. S. Pedersen and W. Richtering, *J. Am. Chem. Soc.*, 2005, **127**, 9372–9373.
15 Y. Umeda, T. Kobayashi, T. Hirai and D. Suzuki, *Colloid Polym. Sci.*, 2011, **289**, 729–737.
16 A. C. Nickel, A. Scotti, J. E. Houston, T. Ito, J. Crassous, J. S. Pedersen and W. Richtering, *Nano Lett.*, 2019, **19**, 8161–8170.
17 S. Wu, J. Dzubiella, J. Kaiser, M. Drechsler, X. Guo, M. Ballauff and Y. Lu, *Angew. Chem.*, 2012, **51**, 2229–2233.
18 J. P. Douliez, A. Perro, J. P. Chapel, B. Goudeau and L. Béven, *Small*, 2018, **14**, 1803042.
19 Y. Han, M. Pan, J. Yuan, S. Mei, L. Zhu, G. Liu and H. Yu, *Nanotechnol*, 2018, **29**, 455602.
20 X. Hu, Z. Tong and L. A. Lyon, *J. Am. Chem. Soc.*, 2010, **132**, 11470–11472.
21 H. F. Ji, X. X. Wang, X. Zhang and X. l. Yang, *Chin. J. Polym. Sci.*, 2010, **28**, 807–817.
22 S. Wu, J. Kaiser, M. Drechsler, M. Ballauff and Y. Lu, *Colloid Polym. Sci.*, 2013, **291**, 231–237.
23 P. Du and P. Liu, *Langmuir*, 2014, **30**, 3060–3068.
24 G. Liu, H. Wang and X. Yang, *Polymer*, 2009, **50**, 2578–2586.
25 G. L. Li, C. A. Tai, K. Neoh, E. Kang and X. Yang, *Polym. Chem.*, 2011, **2**, 1368–1374.
26 L. Zhao, H. Liu, F. Wang and L. Zeng, *J. Mater. Chem. A*, 2014, **2**, 7065–7074.
27 Y. Zhao, T. Chen, S. Sun and L. Zhao, *Adv. Mater. Sci. Eng.*, 2016, **2016**, 2658621.
28 G. Liu, H. Ji, X. Yang and Y. Wang, *Langmuir*, 2008, **24**, 1019–1025.
29 L. Y. Hao, C. L. Zhu, W. Q. Jiang, C. N. Chen, Y. Hu and Z. Y. Chen, *J. Mater. Chem.*, 2004, **14**, 2929–2934.
30 P. Yang, X. Luo, S. Wang, F. Wang, C. Tang and C. Wang, *Colloids Surf., B*, 2017, **151**, 333–343.
31 J. Han, M. Wang, R. Chen, N. Han and R. Guo, *Chem. Commun.*, 2014, **50**, 8295–8298.
32 Y. Du, Z. Huang, S. Wu, K. Xiong, X. Zhang, B. Zheng, R. Nadimicherla, R. Fu and D. Wu, *Polymer*, 2018, **137**, 195–200.
33 M. Zhang, M. Zhu, Y. Zhong, T. Han, B. Sun, S. Zhu, C. Gu, L. Kong, H. Zhang and J. Liu, *Nanotechnol*, 2020, **31**, 455402.
34 R. Begum, Z. H. Farooqi, E. Ahmed, A. Sharif, W. Wu and A. Irfan, *RSC Adv.*, 2019, **9**, 13838–13854.
35 M. Karg, *Colloid Polym. Sci.*, 2012, **290**, 673–688.
36 M. Arif, Z. H. Farooqi, A. Irfan and R. Begum, *J. Mol. Liq.*, 2021, **336**, 116270.
37 C. Echeverria, S. N. Fernandes, M. H. Godinho, J. P. Borges and P. I. Soares, *Gels*, 2018, **4**, 54.
38 Z. H. Farooqi, S. R. Khan, R. Begum and A. Ijaz, *Rev. Chem. Eng.*, 2016, **32**, 49–69.
39 Z. Farooqi, S. Khan and R. Begum, *Mater. Sci. Technol.*, 2017, **33**, 129–137.
40 K. Naseem, R. Begum and Z. H. Farooqi, *Polym. Compos.*, 2018, **39**, 2167–2180.
41 M. Karg and T. Hellweg, *Curr. Opin. Colloid Interface Sci.*, 2009, **14**, 438–450.
42 P. Du, H. Yang, J. Zeng and P. Liu, *J. Mater. Chem. B*, 2013, **1**, 5298–5308.

43 K. Yang, Z. Dai, Y. Chu and G. Chen, *Nano-Micro Lett.*, 2016, **11**, 129–136.
44 G. Li, Q. Shi, S. Yuan, K. Neoh, E. Kang and X. Yang, *Chem. Mater.*, 2010, **22**, 1309–1317.
45 G. Li and X. J. T. Yang, *J. Phys. Chem. B*, 2007, **111**, 12781–12786.
46 S. Wu, J. Dzubiella, J. Kaiser, M. Drechsler, X. Guo, M. Ballauff and Y. Lu, *Angew. Chem., Int. Ed.*, 2012, **51**, 2229–2233.
47 S. Wu, J. Kaiser, M. Drechsler, M. Ballauff and Y. Lu, *Colloid Polym. Sci.*, 2013, **291**, 231–237.
48 P. Du and P. Liu, *Langmuir*, 2014, **30**, 3060–3068.
49 P. Du, H. Yang, J. Zeng and P. Liu, *J. Mater. Chem. B*, 2013, **1**, 5298–5308.
50 L. Liu, J. Zeng, X. Zhao, K. Tian and P. Liu, *Colloids Surf., A*, 2017, **526**, 48–55.
51 L. Liu, P. Du, X. Zhao, J. Zeng and P. Liu, *Eur. Polym. J.*, 2015, **69**, 540–551.
52 J. Li, J. Zeng, X. Jia, L. Liu, T. Zhou and P. Liu, *J. Taiwan Inst. Chem. Eng.*, 2017, **74**, 238–245.
53 G. Nikravan, V. Haddadi-Asl and M. Salami-Kalajahi, *Colloids Surf., B*, 2018, **165**, 1–8.
54 P. Du, T. Wang and P. Liu, *Colloids Surf., B*, 2013, **102**, 1–8.
55 G. Li, C. Lei, C. Wang, K. Neoh, E. Kang and X. Yang, *Macromolecules*, 2008, **41**(23), 9487–9490.
56 X. Yang, Z. Sun, X. Huang, M. Zhang, G. Bian, Y. Qi and X. Yang, *Colloids Surf., A*, 2020, **601**, 124728.
57 M. Kim, K. Sohn, H. B. Na and T. Hyeon, *Nano Lett.*, 2002, **2**, 1383–1387.
58 M. Zhang, Y. Lan, D. Wang, R. Yan, S. Wang, L. Yang and W. Zhang, *Macromolecules*, 2011, **44**, 842–847.
59 L. Liu, J. Guo and P. Liu, *Ind. Eng. Chem. Res.*, 2016, **55**, 4790–4796.
60 K. Kamata, Y. Lu and Y. Xia, *J. Am. Chem. Soc.*, 2003, **125**, 2384–2385.
61 Y. Xu, Y. Yao, H. Yu, B. Shi, S. Gao, L. Zhang, A. L. Miller, J. C. Fang, X. Wang and K. Huang, *ACS Macro Lett.*, 2019, **8**, 1263–1267.
62 F. Wang, J. Liu, D. Wang, Z. Yang, K. Yan and L. Meng, *Nanoscale*, 2019, **11**, 15017–15022.
63 L. Liu, J. Zeng, X. Zhao, K. Tian and P. Liu, *Colloids Surf., A*, 2017, **526**, 48–55.
64 J. Jia, C. Wang, K. Chen and Y. Yin, *Chem. Eng. J.*, 2017, **327**, 953–961.
65 G. Nikravan, V. Haddadi-Asl and M. Salami-Kalajahi, *Colloids Surf., B*, 2018, **165**, 1–8.
66 H. Ji, S. Wang and X. Yang, *Polymer*, 2009, **50**, 133–140.
67 R. Yang, Y. Liu, X. Yan, S. Liu and H. Zheng, *J. Mater. Chem. A*, 2016, **4**, 9807–9815.
68 P. Du, T. Wang and P. Liu, *Colloids Surf., B*, 2013, **102**, 1–8.
69 X. Guo, K. S. González and D. M. Lynn, *Chem. Mater.*, 2019, **31**, 7443–7452.
70 S. Zou, Y. Hu and C. Wang, *Macromol. Rapid Commun.*, 2014, **35**, 1414–1418.
71 G. Liu, H. Wang and X. Yang, *Polymer*, 2009, **50**, 2578–2586.
72 L. Liu, J. Guo and P. Liu, *Ind. Eng. Chem. Res.*, 2016, **55**, 4790–4796.
73 S. Perrier, *Macromolecules*, 2017, **50**, 7433–7447.
74 X. Yang, Z. Sun, X. Huang, M. Zhang, G. Bian, Y. Qi and X. Yang, *Colloids Surf., A*, 2020, **601**, 124728.
75 G. L. Li, C. A. Tai, K. Neoh, E. Kang and X. Yang, *Polym. Chem.*, 2011, **2**, 1368–1374.
76 G. Liu, H. Ji, X. Yang and Y. Wang, *Langmuir*, 2008, **24**, 1019–1025.
77 M. Zhang, Y. Lan, D. Wang, R. Yan, S. Wang, L. Yang and W. Zhang, *Macromolecules*, 2011, **44**, 842–847.
78 Y. Zhao, T. Chen, S. Sun and L. Zhao, *Adv. Mater. Sci. Eng.*, 2016, 2016.
79 L. Zhao, H. Liu, F. Wang and L. Zeng, *J. Mater. Chem. A*, 2014, **2**, 7065–7074.
80 K. Yang, Z. Dai, Y. Chu and G. Chen, *Nano-Micro Lett.*, 2016, **11**, 129–136.
81 C. L. Zhang, F. H. Cao, J. L. Wang, Z. L. Yu, J. Ge, Y. Lu, Z. H. Wang and S. H. Yu, *ACS Appl. Mater. Interfaces*, 2017, **9**, 24857–24863.
82 C. Zhang, Z. C. Yao, Q. Ding, J. J. Choi, Z. Ahmad, M. W. Chang and J. S. Li, *ACS Appl. Mater. Interfaces*, 2017, **9**, 21485–21495.
83 Y. Du, Z. Huang, S. Wu, K. Xiong, X. Zhang, B. Zheng, R. Nadimicherla, R. Fu and D. Wu, *Polymer*, 2018, **137**, 195–200.
84 G. Nikravan, V. Haddadi-Asl and M. Salami-Kalajahi, *Appl. Organomet. Chem.*, 2018, **32**, e4272.
85 B. Liu, X. Yang and H. Ji, *Polym. Int.*, 2010, **59**, 961–966.
86 B. R. Cuenya, *Thin Solid Films*, 2010, **518**, 3127–3150.
87 M. J. Ndolomingo, N. Bingwa and R. Meijboom, *J. Mater. Sci.*, 2020, **55**, 6195–6241.
88 D. Astruc, *Nanopart. Catal.*, 2008, **1**, 1–48.
89 G. Li and Z. Tang, *Nanoscale*, 2014, **6**, 3995–4011.
90 Y. Jia, S. N. Shmakov, P. Register and E. Pinkhassik, *Chem.–Eur. J.*, 2015, **21**, 12709–12714.
91 D. Schmaljohann, *Adv. Drug Delivery Rev.*, 2006, **58**, 1655–1670.
92 N. M. Smeets and T. Hoare, *J. Polym. Sci., Part A: Polym. Chem.*, 2013, **51**, 3027–3043.
93 J. K. Oh, R. Drumright, D. J. Siegwart and K. Matyjaszewski, *Prog. Polym. Sci.*, 2008, **33**, 448–477.
94 C. Zhang, Z. C. Yao, Q. Ding, J. J. Choi, Z. Ahmad, M. W. Chang and J. S. Li, *ACS Appl. Mater. Interfaces*, 2017, **9**, 21485–21495.
95 Z. Shi, Y. Yang, Y. Huang, H. Yue, Z. Cao, H. Dong, Y. Yin and S. Yang, *ACS Sustain. Chem. Eng.*, 2019, **7**, 3995–4003.
96 J. Wang, W. Wang, Y. Zhang, Y. Wang and Y. Zhao, *Nanotechnology*, 2019, **31**, 025403.
97 W. Wei, P. Du, D. Liu, Q. Wang and P. Liu, *Nanoscale*, 2018, **10**, 13037–13044.
98 M. Barakat and E. Schmidt, *Desalination*, 2010, **256**, 90–93.
99 A. Bashir, L. A. Malik, S. Ahad, T. Manzoor, M. A. Bhat, G. Dar and A. H. Pandith, *Environ. Chem. Lett.*, 2019, **17**, 729–754.
100 D. Naghipour, S. D. Ashrafi, M. Gholamzadeh, K. Taghavi and M. Naimi-Joubani, *Data Brief*, 2018, **21**, 1409–1414.
101 Y. Li, Z. Xu, S. Liu, J. Zhang and X. Yang, *Comput. Mater. Sci.*, 2017, **139**, 65–74.
102 A. Pohl, *Water, Air, Soil Pollut.*, 2020, **231**, 503.